Challenge Journal of STRUCTURAL MECHANICS

Vol.5 No.3 (2019)

Mindlin's theory buckling building codes dynamic analysis dynamic response earthquake elastic foundation finite element analysis finite element method nonlinear analysis operational modal analysis optimization prestressing pushover analysis reinforced concrete seismic analysis seismic design seismic isolation soil-structure interaction temperature effects thick plate wind

ISSN 2149-8024

TULPAR ACADEMIC PUBLISHING

Challenge Journal of Structural Mechanics

E-mail: *cjsmec@challengejournal.com*

Web page: *cjsmec.challengejournal.com*

TULPAR Academic Publishing
www.tulparpublishing.com

Challenge Journal of Structural Mechanics

CONTENTS

Research Articles

TULPAR ACADEMIC PUBLISHING

Challenge Journal of Structural Mechanics

Research Article

Utilization of ceramic waste in the production of Khorasan mortar

H. Selim Şengel [a,*], Mehmet Canbaz [a], Ersin Güler [b]

[a] *Department of Civil Engineering, Eskişehir Osmangazi University, 26480 Eskişehir, Turkey*

[b] *Department of Construction Technology, Sivrihisar Vocational School, Eskişehir Osmangazi University, 26600 Eskişehir, Turkey*

ABSTRACT

Khorasan mortar was used in almost all of the historical structures in the geographical area of turkey. It is still used in the renovation of these structures. Water, lime, baked clay is used in the production of Khorasan by breaking and grinding. Crushed brick and tiles are preferred as baked clay. In this study, the usability of ceramic wastes as baked clay was investigated. An important part of ceramic production is made especially in Eskişehir and its vicinity. 10% of ceramic production shows up as wastes because of various reasons. These wastes which are under 20 mm are crushed in the jaw breakers and these which are under 150 mm are grinned in grinders, transformed to powder and then mixed with hydrated lime and water in various proportions, in this way Khorasan mortars are obtained. In mortar production, crushed ceramic-ceramic powder ratio, ceramic-lime ratio were changed and the most suitable ratios were tried to be found. Samples taken from these mortars which are 4 cm x 4 cm x 16 cm in size are removed after a day from the mold and kept in humid environment. Physical and mechanical properties such as unit weight, ultrasonic pulse velocity, bending strength, compressive strength of the mortar were determined. As a result of the experiments, the unit weights range was between 1.5–1.65 kg/dm^3, the ultrasonic pulse velocity rates range from 1.3–1.9 km/h, the range of bending strengths was from 0.25–1.05 MPa, and compressive strength has changed in the range of 7.5–10.5 MPa. With the work done, it is recommended to use a high percentage of lime while using ceramic wastes in the process of producing Khorasan mortar.

ARTICLE INFO

Article history:
Received 22 March 2019
Revised 7 May 2019
Accepted 4 June 2019

Keywords:
Khorasan mortar
Ceramic waste
Bending strength
Compressive strength

1. Introduction

The Khorasan mortar which is prepared by using crushed brick and lime was the most important binding material used in historical structures. Before making any intervention to historical structures, it is necessary to know their characteristics and produce mortar and plaster with these characteristics. Interventions made to historical structures with materials such as cement increase the problems. Therefore, a large number of studies have been carried out on the properties of mortar and plaster used in historical structures (Böke et al., 2004).

The word Khorasan was taken from the Khorasan region in eastern Iran and "Cocciopesto" in the Roman period, "Surkhi" in India, and was named as "Homra" in the Arab countries (Erdoğan, 2003). The Khorasan mortar is often used in the Middle East and Anatolian civilizations where brick structures are very advanced. In the Byzantine, Seljuk and Ottoman structures, there was a wide range of Khorasan mortar usage (Çamlıbel, 1998). The characteristics of the Khorasan mortar are equivalent to today's concrete. Although it is called Horasan but in the study of historical structures, it is stated that the phrase "Khorasan concrete" is more accurate (Akman et al., 1986). Khorasan mortar is a composite of lime, crushed and dust of brick (Özgüleş, 2019). Khorasan mortar as interface material has gained experience in more than ten centuries (Kasimzade et al., 2019a). The studies on the determination of the Khorasan mortar and its properties are still up-to-date (Kasimzade et al., 2019b, Uygunoğlu et al. 2019).

* *Corresponding author*. Tel.: +90-222-239-3750 ; Fax: +90-222-229-0535 ; E-mail address: ssengel@ogu.edu.tr (H. S. Şengel)
ISSN: 2149-8024 / DOI: https://doi.org/10.20528/cjsmec.2019.03.001

Ceramic, by definition, is the process of baking the compounds made with non-organic materials giving them a shape by various methods, with or without glazing until hardening (Thickgrass et al., 2015). Baking can also be defined as the hardness of the formed ceramic under the effect of temperature (Arcasoy, 1983).

In this study, the usability of ceramic wastes as baked clay was investigated. An important part of ceramic production is made especially in Eskişehir and its vicinity. 10% of ceramics production shows up as wastes because of various reasons. These wastes which are under 20 mm are crushed in the jaw breakers, these which are under 150 mm are grinned in grinders and transformed to powder, then mixed with hydrated lime and water in various proportions, in this way Khorasan mortars are obtained. In mortar production, crushed ceramic-ceramic powder ratio, ceramic-lime ratio was changed and the most suitable ratios were tried to be found. The study showed that ceramic wastes can be used in the production of Khorasan mortar. However, in order to use ceramic wastes in the production of Khorasan mortar, it should be determined not only mechanical and physical properties but also durability properties.

2. Materials and Experimental Method

Hydrated lime: The bagged powder lime which was produced by Adaçal A.Ş. in which the calcium lime in the structure of the extinct limestone is 80 and suitable with the TS EN 459-1 is used. Chemical properties are given in Table 1.

Table 1. Chemical properties of hydrated lime.

Active $Ca(OH)_2$, %	Humidity, %	SiO_2, %	MgO, %	SO_3, %	R_2O_3, %
80-85	0.5-1	0-0.1	0.2-0.4	0.1-0.3	0.1-0.2

Crushed ceramic and powder: Crushed ceramics used in the experiments were obtained from the ceramics produced by Eczacıbaşı Vitra Artema Bilecik Bozüyük factory. They are broken up to 20 mm in size in Jaw crushers. In order to obtain the ceramic powder, these crushed particles which were milled in a ball mill were sifted by a 150 mm sieve. Chemical properties of ceramic wastes are given in Table 2.

Table 2. Chemical properties of ceramic waste.

Content	%	Content	%
SiO_2	63.45	CaO	8.18
Al_2O_3	13.98	Na_2O	0.90
Fe_2O_3	5.39	K_2O	2.43
TiO_2	0.77	SO_3	0.10

In the production of Khorasan mortar, 0-2 cm crushed ceramic and 0-150 cm ceramic powder are used as crushed baked clay and powder. Hydrated lime is used as lime. The mixing ratios are given in Table 3. 4 cm x 4 cm x 16 cm specimens were taken from the produced Khorasan mortar. After 1 day, specimens removed from their molds were covered with wet cloth. The cloth is kept wet by occasional soaking. After 7 and 28 days of production, the physical and mechanical characteristics such as unit weight, ultrasonic, bending and compression tests were carried out, and as a result the unit weight of the mortar, ultrasonic transition velocity, bending strength, compressive strength were determined.

Table 3. Mixing ratios.

Crushed ceramic, gr	Ceramic powder, gr	Water, gr	Hydrated lime, gr	Baked clay powder/lime
800	800	800	400	2
800	600	800	600	1
800	400	800	800	0,5

3. Results and Discussions

Fig. 1 shows the change in the unit weights of the Khorasan mortar produced with waste ceramics. In Fig. 1, when the ceramic powder-lime ratio increased in 7-day samples, the unit weight decreased by 2%, While in the 28-day specimens increased by 2% and decreased by 3% at higher ratios. In general, it was noticed that the 28-day specimens have higher unit weights. Also the addition of ceramic dust decreased the unit weight, as the density of the ceramics was much lower. Since the shrinkage of specimens is higher in older ages, the unit weight increases a little bit as their ages increase too.

In Fig. 2, the changes in ultrasonic pulse velocity are observed depending on the ceramic powder-lime ratio of the Khorasan mortar. In Fig. 2, when the ceramic powder-lime ratio increases, the ultrasonic pulse velocity increases by 15% in the 7-day samples, while the 28-day samples increases by 4%. As the increase of ceramic dust increases the amount of silicate, aluminate and iron in the environment, the compounds that can react with the lime have increased, so that the increase in the compactness increases the ultrasonic pulse velocity. In addition, it's noticed that the ultrasonic pulse velocity of the 28-day specimens is higher than the 7-day specimens by about 30%. This suggests that the products of hydration reactions continue to increase in the compactness of the microstructure, thereby increasing the ultrasonic pulse velocities.

Fig. 3 shows the change in values of the dynamic elastic modulus obtained depending on the unit weight and the ultrasonic pulse velocity of the samples. When examining Fig. 3, the increase of ceramic powder in 7-day samples increased the dynamic elasticity modules by

around 30%, while it increased by only 6% in 28-day samples. This increasing rate decreases as the ceramic powder and lime's hydration reaction speed decreases in advanced ages. The dynamic elasticity modules of the 28-day specimens showed an increase of 90% compared to the 7-day specimens. This increase rate has increased, especially since the change in unit weight and ultrasonic pulse velocity is evaluated together.

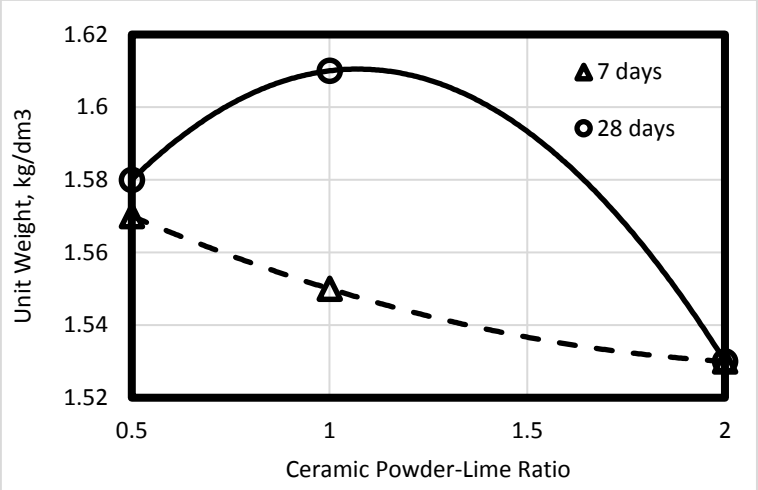

Fig. 1. Unit weight values of specimens.

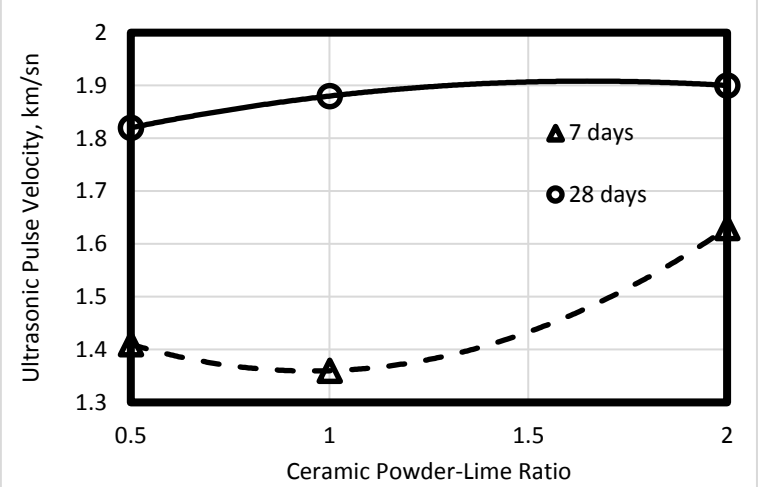

Fig. 2. Ultrasonic pulse velocity values of the specimens.

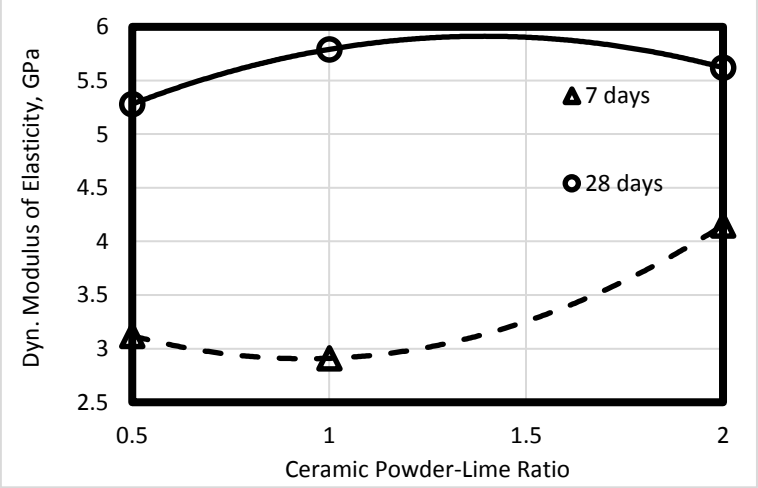

Fig. 3. Dynamic modulus of elasticity values of specimens.

Fig. 4 shows the change in bending strength of the Khorasan mortar produced with ceramic wastes. As the ceramic powder increased in 7-day samples when examined in Fig. 4, there was no remarkable +1% change rate in the bending strength. However, in 28-day samples, the increase in ceramic dust-lime ratio increased the bending strength by 9%. From that it can be said that the reactions made by the ceramic powder fill the gaps in the microstructure and As a result of obtaining more filled sections the bending strength increases. It is observed that only 30% of the 28-day bending strength can be reached at early age.

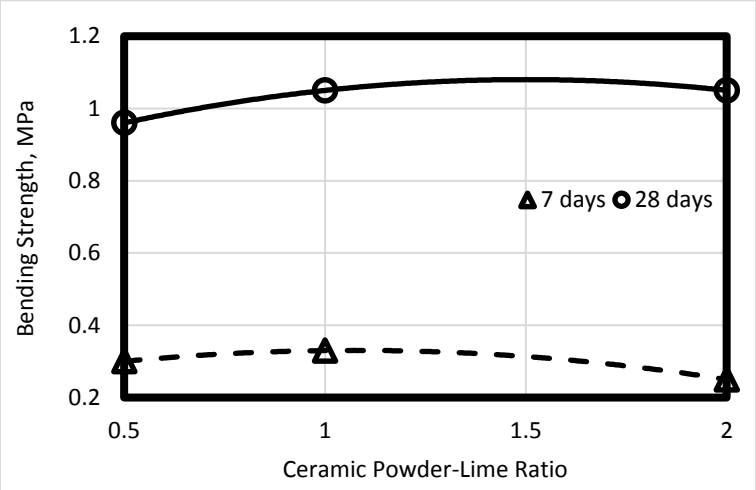

Fig. 4. Bending strength values of samples.

In Fig. 5, it's observed that the change of compressive strength depends on the ceramic dust-lime ratio of the Khorasan mortar. In Fig. 5, the increase of ceramic powder increases the compressive strength by up to 7% in 7-day samples. In 28-day samples, the ceramic powder-lime ratio was 1 and increased by 11% compared to the other ceramic powder-lime ratios. In terms of strength, the ideal ceramic powder, lime mixing rate is 1. Considering the Time-dependent strength development, it has been observed that about 80% of the 28 days compressive strength values are achieved in 7 days. At an early age, significant values such as 8 MPa were reached, while in 28 days the ceramic powder-lime ratio was 1, and compressive strength values exceeding 10 MPa were observed.

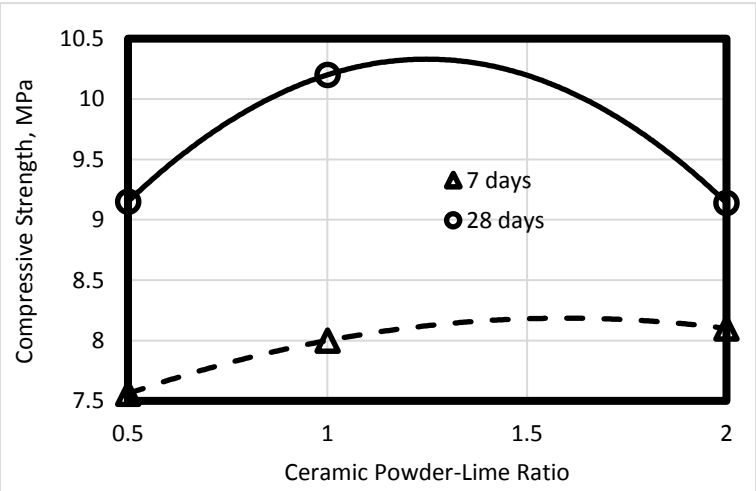

Fig. 5. Compressive strength values of specimens.

4. Conclusions

The following results have been achieved in the study on the evaluation of ceramic wastes.

- In the 7-day samples, with the increase of ceramic powder in the mixture, the unit weights decreased by 2%, ultrasonic pulse velocities increased by 15%, dynamic elasticity modules increased by 30%, compressive strength increased by 7% and there was no significant change in bending strength.
- In the 28-day samples, when the ceramic powder-lime ratio increased from 0.5 to 1, the unit weights increased by 2%, ultrasonic pulse velocities increased by 4%, dynamic elasticity modules increased by 6%, bending strength by 9%, compressive strength by 11%. The physical and mechanical properties of the

specimens were either unaltered or negatively affected when the ceramic powder-lime ratio increased from 1 to 2.

- When the change in the characteristics of age-related specimens is examined, it has been observed that the unit weights, ultrasonic pulse velocities, dynamic modulus of elasticity, bending and compressive strength of specimens have increased over time. Especially the increase in bending strength has reached up to twice the strength of early age.

The study showed that ceramic wastes can be used in the production of Khorasan mortar. Especially the ceramic powder-lime ratio mixtures can be suggested as 1. The compressive strength, which is characteristic for brittle materials, has passed 10 MPa for the ceramic powder-lime ratio 1. It should be kept in mind that the effect of ceramic wastes on the durability of Khorasan mortar should also be determined before being evaluated in the production of Khorasan mortar.

REFERENCES

Akman MS, Güner A, Aksoy İH (1986). The history and properties of Khorasan mortar and concrete. Turkish and İslamic Science and Technology in the 16th Century, I: 101-112.

Arcasoy A (1983). Ceramic Technology. Marmara University Publications, Publication No: 457.

Böke H, Akkurt S, Ipekoğlu B (2004). The properties of Horasan mortar and plasters used in historical buildings. *Yapı Magazine,* 269, 90-95.

Çamlıbel N (1998). The Analytical examination of structures in Sinan's architecture. Yıldız Technical University Printing Publishing Center, Istanbul.

Erdogan TY (2003). Concrete. METU Development Foundation Publication and Communication Inc., Ankara.

Kalınçimen G, Öztürk AU, Kaplan G, Yıldızel SA (2015). Use of ceramic wastes as cement substitution material and examination of acid endurance. *Kastamonu University Journal of Engineering and Sciences*, 1(1), 9-16.

Kasimzade AA, Dushimimana A, Tuhta S, Atmaca G, Günday F, Abrar O (2019a). A comparative study on effectiveness of using Horasan mortar as a pure friction sliding interface material. *European Journal of Engineering Research and Science*, 4(2), 64-69.

Kasimzade AA, Tuhta S, Atmaca G (2019b). Horasan Mortar Bearings in Base Isolation with Centuries Experiences. In Seismic Isolation, Structural Health Monitoring, and Performance Based Seismic Design in Earthquake Engineering. Springer, Cham, 85-127.

Özgüleş M (2019). Archival Documents as Sources of Historic Structures' Construction Materials and Technique: Three Case Studies from Ottoman Architecture. *In Structural Analysis of Historical Constructions*. Springer, Cham, 1979-1987.

Uygunoğlu T, Topçu İB, Çınar E, Resuloğulları D (2019). Electrical and mechanical properties of historical mortars in Bursa/Turkey. *Revista de la Construcción. Journal of Construction*, 18(1), 54-67.

Challenge Journal of Structural Mechanics

Research Article

The impact of design approach and contracting practices on cost and execution period of school buildings

Abdullatif A. AlMunifi [a,b], Ibrahim Abdullah Alameri [a,*]

[a] *Department of Civil Engineering, Faculty of Engineering, Sana'a University, Sana'a 13341, Yemen*
[b] *Department of Civil Engineering, Unaizah College of Engineering, Qassim University, Unaizah 56452, Saudi Arabia*

ABSTRACT

More than two million school-age children in Yemen are unable to enroll in education because of a shortage of school buildings. This is one of the reasons the country missed the Millennium Development Goal of achieving Education for all by 2015. The struggle to afford school accommodation will continue, because of the lack of resources and high unit cost. Construction cost as time schedule for an identical school building vary by the implementing agency. This paper aims to study in-depth this multi-dimensional issue to find out the factors that lead to this variation, as well as the reasons for the high unit cost and lengthy periods of construction. To achieve this objective, comprehensive raw data that was resourced from agencies that are assigned to implement the largest part of the construction program along with data collected through questionnaires and semi-structured interviews were utilized. Complete sets of design and contracting documents of representative schools were used for deeper analysis and evaluation. The analysis shows that the employed design approaches lead to large structural elements and consequently to longer implementation period and 30% increase in cost. It also shows that contractors add up to 20% for the client's procurement procedure, approvals, and payment cycle. Additionally, bidders price risks related to accessibility to building sites, availability of building materials, and how trouble-prone is the region. The findings are of relevance to researchers, education planners, and practitioners as they are of high importance to policy makers and financiers whose main concern is to meet the growing need for school accommodation.

ARTICLE INFO

Article history:
Received 5 April 2019
Revised 15 June 2019
Accepted 12 July 2019

Keywords:
Design and procurement practices
Bid and risk-based pricing
Out-of-school children
Yemen

1. Introduction

Yemen is among the poorest countries in the world and is the poorest country in the Middle East (The World Bank, 2013). Yemen is a mountainous country with more than 75% of the 25 million population scattered in more than a hundred thousand of tiny settlements that are built in very rugged and inaccessible mountains. This habitation pattern imposes serious constrains in achieving developmental plans (AlMunifi, 1997).

Recognizing education to be one of the key factors in reducing poverty and promoting economic development, the Government has committed to give a high priority to the education as a fundamental tool to the development of the country. The Article (54) of the Yemen Constitution states the following "Education is a right for all citizens, and basic education is obligatory" (Yemeni government, 2018). The government also is committed to meeting the Millennium Development Goals (MDGs). Specific targets that are linked to the MDGs in primary education outlined in the Country Proposal to the Education for All Fast Track Initiative (EFA FTI) (Khan and Chase, 2003). Five major national strategies were endorsed to address education issues. The Basic Education Development Strategy (BEDS) 2003–15 aims to increase enrollment in basic education to reach 95-100 percent by 2015 (Brown, 2013).

* *Corresponding author*. E-mail address: i.ameri@eng-su.edu.ye (I. A. Alameri)
ISSN: 2149-8024 / DOI: https://doi.org/10.20528/cjsmec.2019.03.002

2. Background of the Problem

Yemen has low basic enrollments (60% GERs), and high population growth, at 3%, the number of out-school children will peak at 2020 and a 3.7 million children ages 6-15 will lack a place in school, Fig. 1 (The World Bank, 1999).

Given the above-mentioned facts, a considerable deficit of nearly 80,000 classrooms remains for Yemen to achieve 100% GERs in basic education. The Quantitative requirements for basic education for all are shown in Fig. 2 (The World Bank, 1999).

In 2013, the Ministry of Education (MOE) developed a Mid Term Results Framework (MTRF), which informed the achievement of 87% Gross Enrolment Rate (GER) toward Universal Primary Education. The MOE projected to achieve 89.3% (GER) in basic education by 2015. However, the MTRF emphasizes the structural challenges that the education sector faces including lack of school buildings, and lack of resources that totaled up to US$ 4.0 Billion. The MTRF concluded that Yemen is unlikely to achieve the MDG of Education for All by 2015, given that only 87% of children are enrolled in schools in 2013 (MOE, 2013).

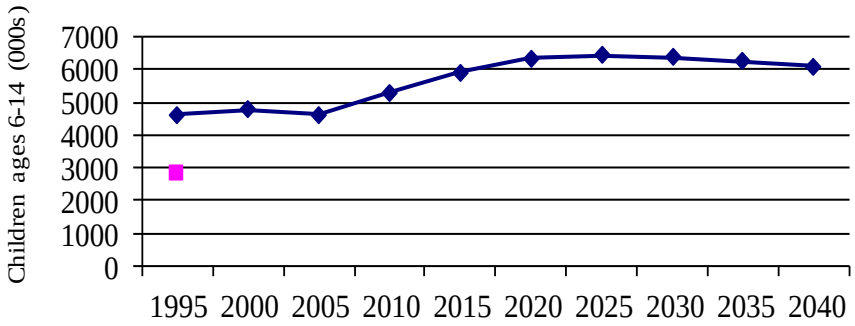

Fig. 1. The number of out-school children, World Bank staff estimates using data from 1994 Population Census 1997 DHS.

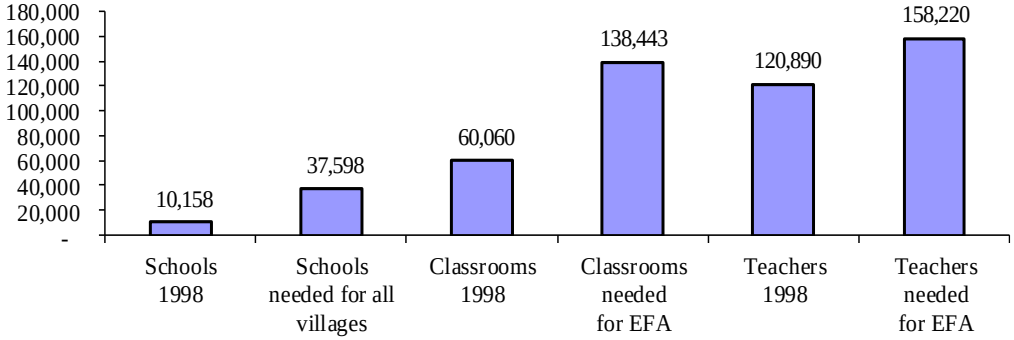

Fig. 2. The quantitative requirements for basic education (The World Bank, 1999).

There is a shortage of classrooms particularly in rural areas, where 28% of out-school children reported that they were not enrolled in school because there was no school close by or because travel to the local school was too difficult (Brown, 2013). The situation became alerting with the break of war in 2015 and escalating violence over the past four years. More than 2,500 schools are out of use. 66% were damaged by the heavy violence, 27 have closed down, and 7% used to shelter displaced families or for military purposes. This has disrupted children's schooling and contributed to a 20% increase in the number of out-of-school children, from 1.6 million before the war to 2 million today (UNICEF, 2018).

To accommodate out-of-school population, it will require significant investments and tangible reform in school construction program in term of school design approaches and contracting practices. AlMunifi (2004) stated that to support the MOE in expanding access, the World Bank-Government financed-projects allocated nearly 70% of the resources to increase the number of classrooms for students in critically deficient areas.

The need is huge in the very normal situation without taking into consideration the effects of the ongoing war on school buildings. The MOE should afford to add annually approximately 12000 classrooms to accommodate out-of-school children. This is an increase of 50% of the annual plan and current capacity production. A set of policies such as, building new classrooms based on school mapping, rehabilitating unserviceable schools, and improving mechanisms for routine maintenance of existing schools, should be in-place, and be accompanied with a program to strengthening the capacity of the MOE in school construction.

The war has caused a serious deterioration of the economic and social conditions in the country; nevertheless, education will continue to be the cornerstone to rebuild the country given that 50% of Yemen's population is under the age of 18.

3. Literature Review

Despite that high cost of school construction is a hot topic and is making headline in the country, a very limited research work has been conducted in this aspect. There is a lack of background research papers in the subject area and about the country of interest in particular. Most of the available reports and researches are focused on comparing delivery cost of a classroom among different implementing agencies; And those with further details, the value of school contract divided by the gross built area to get the cost per square meter. Without giving attention to the big variations in the components of schools, the distance and accessibility to building sites, urban-rural, and types of construction material. The impact of design approach and most importantly the regulations and contracting practices that are followed by the implementing agencies have not yet been given any attention.

A direct cost comparison between different school types built by the various implementation agencies is difficult if not even impossible. Some implementing agencies are mainly active in rural areas, other in both rural and urban. The working paper: Yemen Experience with the Fast Track Initiative that presented in the Fast Track Initiative Partnership Meeting in Brasilia in 2004 shows that the variations in costs of school construction in two governorates hit the range of US$15000 to US$19000 per classroom (Fast Track Initiative, 2004). Yet, what factors led to such variation.

The MOE, in the context of preparing school construction plans and policies, conducted in 2004 school construction cost analysis for projects implemented between 1997 and 2002. The outcome of the analysis is US$146/sq. m. This was considered as good basis for 2004 with estimated inflation rates of the Yemeni construction sector (MOE, 2004).

Ogawa, K (2004) in his task to assess school construction costs to estimate the financing requirement to achieve Universal Primary Education reviewed school construction in Yemen. He found the unit cost of classroom varies from US$5,000 (UNICEF), between US$10,044 and US$12,171 (SFD, PWP, BEEP), between US$14,000 and US$16,000 (the Ministry of Education), to US$26,000 (Japan). He assumed that the difference in costs depends on school design, type of construction, and administrative procedures. Nevertheless, comparing to other countries he found that the unit cost in Yemen is very high-US$3,100 in India, US$3,900 in Bangladesh; US$4,700 in Mauritania; US$7,500 in Guinea; US$8,200 in Brazil; and US$10,000 in Mexico (Ogawa, 2004).

As far as the authors are aware, the tendering procedure for Japan supported school construction program took place in Japan with participation of only Japanese contractors who in their turn subcontracted local constructors. Therefore, the very high unit cost is justifiable.

The WB & YG Mission Report (2005) Reviewed civil works components in four education projects. They found that the very low unit cost per classroom in the Child Development Project implemented by UNICEF is mainly due to the lack of other facilities than classrooms in most of the new schools. In addition, the dimensions of classrooms are smaller, and built by small contractors who are contracted by local communities. With the addition of new facilities to the initial standard design, the unit costs will probably increase up to US$10,000. The report concluded that a comparison between different designs would be more accurate by square meter in gross area (The World Bank & Yemen Government, 2005).

Döring, (2010) attempted to identify solutions to reduce the cost of school construction. He avoided comparing the unit cost of different school types erected by the various implementation agencies. His work based on the assumption that there should be minimum requirements set for a school to be regarded as being "fully functional". The study concluded that there has an overall potential for cost reductions of up to 25% compared to current practices, combining a series of short-term improvements with a set of long-term capacity building measures (Döring, 2010).

The delivery system in school construction sector differs by implementing agency. Each has its procurement framework, procedures and disbursement flow. This variation in procurement procedures and disbursement arrangements reflects the procurement guidelines of the financier.

The Law No. 23 for 2007 on Tenders, Auctions, and Government Storehouses regulates the public procurement in the country. All government entities, ministries, and corporations should refer to this legal framework and must use Standard Bidding Documents to carry out any procurement activity (National Info. Centre, 2018).

The MOE has an accumulated procurement experience practicing the Government Procurement Law, as a government entity. It has been the main implementing agency for school buildings. The procurement methods used for the procurement of construction services is mainly National Competitive Bidding and is used for all types and sizes of schools. It is a practice that payment certificates take time to be processed and approved, and a very long time to be disbursed.

The PWP and the SFD are covering all the Country Governorates in both rural and urban areas. The two agencies are funded by a number of donors with a World Bank lead. Based on The PWP and the SFD long and successful experience in administering school construction programs and public works in general, they have developed a Simplified Standard Bidding Documents for Works. The standard size of schools is different for each project. The SFD project has ten different standard schools corresponding to rural or urban areas, number of floors (one to three floors) and number of classrooms or half classrooms (3 to 36). The PWP has also ten standard schools with only 3, 6, or 12 classrooms or half classrooms. (SFD 2018 and PWP, 2018).

Both agencies are governed by the procurement guidelines of the financiers that are documented in the Credit Agreements as in the Projects documentation. The two agencies procurement procedures are much shorter comparing to the MOE that follows the government extended regulations. MOE Reports have shown that the two agencies, the PWP and SFD, have a good reputation with contractors as reliable contract partners with streamlined processing of decisions and most important fast payment cycles on delivered works (Ministry of Education, 2003).

Vincent and Monkkonen (2010) studied the impact of state regulations on the costs of public-school construction. They have measured the impacts of three regulations on the costs of construction and found that states with all three regulations have construction costs that are roughly 30% higher than states with none of the three regulations. AL-Kohlani, (2009) found that SFD and PWP have good procedure in place that ensures securing projects funds before the tender and making payments on time. Therefore, contractors trust these two agencies and do not seriously consider issues related to delay in payments. Zaghloul, and Hartman, (2003) indicated that a trust relationship between the contracting parties should exist first. This can be done through a clear understanding of the risks being born by each party and can result in cost saving in the construction industry.

4. Research Questions

This paper is addressing the high cost of investment in school construction program. The main objective of our research is to analyze to what extent the design approach as well as the contracting practices impact the school construction cost and time schedule. To accomplish this objective, the following questions are to be answered:

Does the design approach have an impact on cost and execution period of school Building?

Do the contracting practices have an impact on cost and execution period of school Building?

5. Research Contribution to Knowledge

Many developing countries struggle to afford the required infrastructure for the increasing school-age population. The analyses and findings of this research would enrich the knowledge and would serve as a tool in the hands of education planners, practitioners, policy makers, and financiers to meet the growing need for school accommodation. It is also a challenge for researchers for further research to study the impacts of risks related to accessibility to building sites, distance from asphalt roads, availability of building materials, and how trouble-prone the region is.

6. Research Methodology

After an extensive and thorough review of relevant documents and the authors' archive with a good number of unpublished reports and communications, the researchers decided to adopt a combination of qualitative and quantitative methods. Targeted groups were identified, namely: individual designers, engineering consulting firms, administrative and procurement staff, contractors, site supervisors, and financial staff. Short questionnaires were structured to collect data from each targeted group.

To elaborate more on the responses obtained from the questionnaires, semi-structured interviews were conducted. This enabled the researchers to get in-depth responses, and to reach key senior staff that usually are either busy to respond to questionnaires or their responses were not considered carefully.

Designers were targeted with questions to get information about design approach, used building codes, combination of design loads, soil investigation, and site conditions.

Administrative and procurement staff were targeted with questions related to tenders preparation, initial cost estimates and budget allocation, bid solicitation, bids evaluation and contract awarding.

Contractors were targeted with questions to get information on how they take the decision to participate in a bidding process, how they prepare bids in term of cost estimate and calculation of indirect cost, and profit, and how specifically they price risks.

Site Engineers were targeted with questions to get information about their duties, rights, and payment terms. Are they conducting works according to contractual terms and following contractors' works to ensure execution according to specifications and time schedule? Are there any grey areas that allow any for any misconduct?

Very valuable data were received from all parties. The analysis of the data shows that each agency has its own procurement procedure and follows different design approach. Therefore, the researchers moved further and acquired complete sets of contractual documents for a number of schools to study and analyze in-depth.

For the purpose of this study, five schools (3 rural and 2 urban) that are financed by the three school implementing agencies, namely, Social Fund for Development (SFD), Public Work Project (PWP), and the MOE, and have full sets of contractual documents available were selected. The schools were contracted and implemented in 2013 (before the break of war in 2015).

Taking into account the repetitive procedures, the researchers consider the sample as adequate and very representative. Full analysis of designs and contractual documents was carried out. Cost estimate was conducted according to the market price. Indirect costs were considered.

7. Design Approach

Based on the analysis of data collected from questionnaires and interviews, and after studying the school design documents and drawings, it was found that all the three agencies used Working Stress Method for structural design. This leads to an exaggeration in the dimensions of structural elements, and consequently larger quantities of concrete and reinforcing steel.

It was found that there is an overestimation in the presumption of live loads applied to the school buildings, especially by the MOE and PWP designers. Soil investigation and site topography and conditions are neglected in the design, which leads to variation orders that resulted in cost, and schedule overruns. Günhan et al. (2007) outlined in their study that is of relevance to practitioners involved in school design and construction projects that the large number and magnitude of change orders in projects constitute an impediment to the rapid and economic delivery of these projects. They found from the analysis of

a large number of change orders in school projects that the school projects can be completed with change orders not exceeding 5% of the contract value. This is valid if measures such as: choosing the right construction management firm, emphasizing the definition of project scope early in the project, and effectively managing the pre-contract activities by conducting value engineering and constructability reviews, Günhan et al. (2007).

The five schools were redesigned using the Ultimate Stress Method, and quantities of concrete and steel of the main structural elements were compared to the available designs as shown in Tables 1 to 10.

Table 1. Amount of concrete in S1 School.

Quantities of concrete (m^3) in main structural elements			
School Code	S1 (Three-Story Building)		
Structure Member	SFD Design	Re-Designed by USM	Percentage of saving in m^3
Footing	91	59	35%
Columns	54	49	9%
Ground Beams	21	17	19%
Beams	94	71	24%
Slabs	102	102	0%
Lintel	10	10	0%
Stairs	12	12	0%
Total	384	320	17%

Table 2. Amount of steel reinforcement in S1 School.

Quantities of steel reinforcement (kg) in main structural elements			
School Code	S1 (Three-Story Building)		
Structure Member	SFD Design	Re-Designed by USM	Percentage of saving in kg
Footing	5848	4333	26%
Columns	12086	8009	34%
Ground Beams	2647	2029	23%
Beams	15085	11151	26%
Slabs	13540	10155	25%
Lintel	1437	1437	0%
Stairs	1050	840	20%
Total	51693	37954	27%

Table 3. Amount of concrete in S2 School.

Quantities of concrete (m^3) in main structural elements			
School Code	S2 (Three-Story Building)		
Structure Member	PWP Design	Re-Designed by USM	Percentage of saving in m^3
Footing	46	25	46%
Columns	29	24	17%
Ground Beams	8	7	13%
Beams	57	30	47%
Slabs	47	47	0%
Lintel	8	7	13%
Stairs	12	10	17%
Total	207	150	28%

Table 4. Amount of steel reinforcement in S2 School.

Quantities of steel reinforcement (kg) in main structural elements			
School Code	S2 (Three-Story Building)		
Structure Member	PWP Design	Re-Designed by USM	Percentage of saving in m^3
Footing	3919	2118	46%
Columns	5635	4620	18%
Ground Beams	882	646	27%
Beams	8813	4793	46%
Slabs	7366	5565	24%
Lintel	820	656	20%
Stairs	2011	1900	6%
Total	29446	20298	31%

Table 5. Amount of concrete in S3 School.

Quantities of concrete (m^3) in main structural elements			
School Code	S3 (Two-Story Building)		
Structure Member	MOE Design	Re-Designed by USM	Percentage of saving in m^3
Footing	56	34	39%
Columns	27	21	22%
Ground Beams	22	17	23%
Beams	53	30	43%
Slabs	48	48	0%
Lintel	5	4	20%
Stairs	12	8	33%
Total	223	162	27%

Table 6. Amount of steel reinforcement in S3 School.

Quantities of steel reinforcement (kg) in main structural elements			
School Code	S3 (Two-Story Building)		
Structure Member	MOE Design	Re-Designed by USM	Percentage of saving in m^3
Footing	3166	2513	21%
Columns	3788	3487	8%
Ground Beams	2016	1540	24%
Beams	8283	3705	55%
Slabs	6227	4731	24%
Lintel	516	516	0%
Stairs	700	570	19%
Total	24696	17062	31%

Table 7. Amount of concrete in S4 School.

Quantities of concrete (m^3) in main structural elements			
School Code	S4 (Two-Story Building)		
Structure Member	PWP Design	Re-Designed by USM	Percentage of saving in m^3
Footing	188	82	56%
Columns	76	52	32%
Ground Beams	40	27	33%
Beams	99	81	18%
Slabs	104	104	0%
Lintel	9	8	11%
Stairs	12	11	8%
Total	528	365	31%

Table 8. Amount of steel reinforcement in S4 School.

Quantities of steel reinforcement (kg) in main structural elements			
School Code	S4 (Two-Story Building)		
Structure Member	PWP Design	Re-Designed by USM	Percentage of saving in m^3
Footing	14950	6424	57%
Columns	14855	9758	34%
Ground Beams	7225	3607	50%
Beams	20450	12914	37%
Slabs	12942	11742	9%
Lintel	1902	1202	37%
Stairs	2112	1998	5%
Total	74436	47645	36%

Table 9. Amount of concrete in S5 School.

Quantities of concrete (m^3) in main structural elements			
School Code	S5 (Three-Story Building)		
Structure Member	SFD Design	Re-Designed by USM	Percentage of saving in m^3
Footing	170	119	30%
Columns	123	114	7%
Ground Beams	54	40	26%
Beams	224	180	20%
Slabs	264	211	20%
Lintel	14	12	14%
Stairs	22	19	14%
Total	871	695	20%

Table 10. Amount of steel reinforcement in S5 School.

Quantities of steel reinforcement (kg) in main structural elements			
School Code	S5 (Three-Story Building)		
Structure Member	SFD Design	Re-Designed by USM	Percentage of saving in m^3
Footing	11857	9353	21%
Columns	29846	23739	20%
Ground Beams	7445	7225	3%
Beams	36770	28415	23%
Slabs	32027	19725	38%
Lintel	3450	2890	16%
Stairs	4276	3895	9%
Total	125671	95242	24%

Examining the quantities of concrete and steel that resulted from redesigning schools, it shows that are much less comparing to the contracted quantities by the MOE and PWP. The SFD is doing better and this is justifiable. As stated earlier, the three agencies use the WSM for design. Moreover, the MOE and PWP adopt large live loads, while the SFD refers to the Uniform Building Code to estimate the live load.

In Summary, the quantities of concrete would be reduced by 17 to 31%, and the quantities of steel reinforcement would be reduced by 24 to 36%, if the implementing agencies changed the design approach, as shown in the following Figs. 3 and 4.

8. Contracting Practices

The contractual practices that are followed by client play a major role in bids pricing. A lengthy procurement and less transparent procedure, and payments delay lead to a 40% increase in bid proposal. This case was registered for an identical project in which two proposals were submitted to two different implementing agencies by the same contractor (Authors' archive).

9. Procurement Procedures

The procurement procedures that are practiced by the three agencies were reviewed.

It is a mandatory for the MOE, as a government entity, to practice the government procurement law, which involves lengthy procedures. It seems that they were doing well, but with the pass of time and the appearance of new competitive implementing agencies, it became clear that the MOE tendering process is very lengthy and less transparent. There is also an extensive decentralization and delegation of authorities to lower governorates level, where technical capacities are minimal. In addition, interventions of influential people are badly influencing the process.

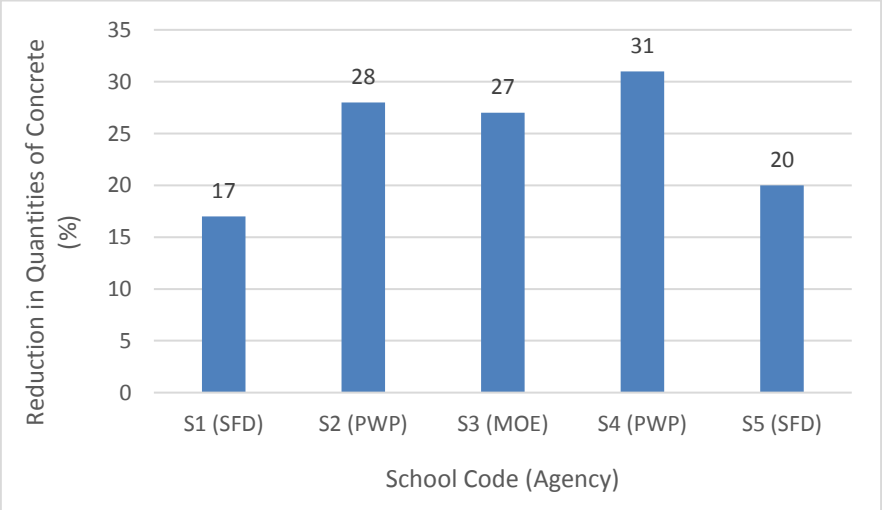

Fig. 3. The reduction percentage in quantities of concrete between agencies' designs and re-design by USM.

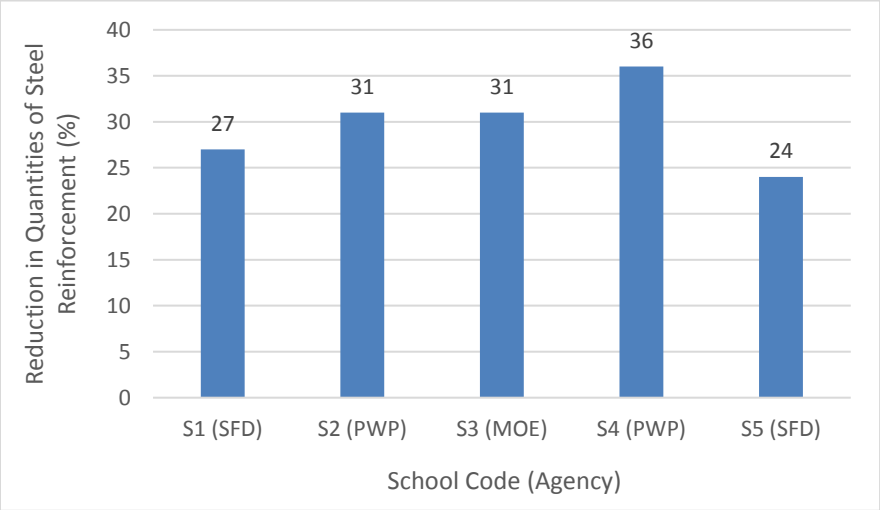

Fig. 4. The reduction percentage in quantities of steel reinforcement between agencies' designs and re-design by USM.

The delay in processing payment certificates is also one of the factors that have serious impact in bidder decision, and contractors usually price the risk of payment delays. It is a typical practice, that the procurement and financial departments request a long list of documents to activate payments to contractors. These documents differ according to the construction phase and are to be endorsed by various authorities and attached to any claim. It is quite an exhausted procedure for contractors for which they make up their calculations. As a result, contractors working for the MOE are consistently late in delivering projects and in particular if they are not technically and financially capable.

The PWP and the SFD have been established as part of the country financial and administrative reform program. They are impermanent structures that are staffed with competitively recruited staff. The remunerations of their staff are much higher than the government staff and usually covered from credits and grants. These two agencies carry out their procurement activities in accordance with the World Bank guidelines for Works. They also respect other donors procurement guidelines wherever and whenever is required. They have competitive and well-experienced management. This is supported by consulting engineers, well-performed contractors, and well-established local units that spread over all the country. Consequently, the procurement procedures and approval requirements are shorter with limited cycle of approvals comparing to the MOE.

Analyzing the collected data relevant to contracting processes, from tender announcement until the project handing over, it was found that: the SFD given 9 out of 10, the PWP given 8 out of 10 and the MOE given 6 out of 10, as shown in Fig. 5.

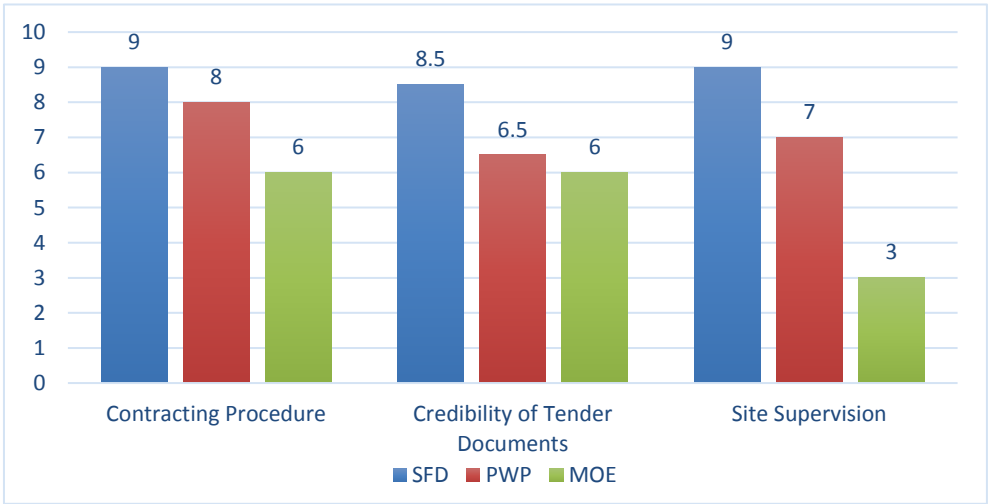

Fig. 5. Contracting process, credibility of tender documents, and site supervision for the three agencies.

10. Tender Documents Credibility

There are also other factors influencing bids costing as how clear and credible are the designs, bills of quantities, and technical specifications. There is a big doubt about the accuracy of the tender documents contents. Dosumu (2018) investigated the prevalent errors in contract documents and their effects on construction projects. The results indicate that errors in contract documents were moderately prevalent. However, over

measurement in bill of quantities was prevalent in private, institutional and management procured projects. Drawings contain the highest number of errors, followed by bill of quantities and specifications.

The contractors price this risk according to their experience with the implementing agency. Laryea and Hughes (2008) studied the complex relationship between risk and price in the bidding practices of contractors. They found that contractors select projects carefully in order to avoid unnecessary tendering costs and determine the appropriate risk to price, negotiate, or avoid. It was found that the SFD tender documents are more reliable and rated 8.5 out of 10, the PWP 6.5 and the MOE 6.

11. Site Supervision

Another factor that is worrying the contractors is the site supervision and follow-up by client engineer, which is connected to immediate solving of any problems that may arouse. Much more important is, the existence of an engineer supervisor to facilitate and approve payment certificates on time. The SFD is doing very well by assigning supervisors to construction sites. They got 9 of 10 comparing to only 3 given to MOE and 7 to PWP, as shown in Fig. 5.

Laryea and Hughes (2008) describing how trust and relationships influence prices, they found that most contractors would offer a certain, favorable level of prices to a client with whom they have a previous positive relationship.

12. Conclusions

In view of the accumulated challenges, it has become necessary to adopt a set of policies that are based on the best practices in school construction. This work is an attempt to put a cornerstone and open the doors for further discussions and research to investigate the main reasons and factors that are affecting the cost and execution period of school buildings.

The scope of this research is limited to areas where immediate steps can be taken to improve the sector performance. Therefore, the study handled the two most influential dimensions of the problem and did not go further to list all playing factors, because a number of those listed as problems are in fact environmental and few things can be done to alter.

Accommodating the out-of-school population requires significant investments and reform in school construction program in term of school design approach, procurement procedures, contracting practices, sites supervision, and payments processing. From the analysis, it was found that the delivery system in school construction sector differ by implementing agency. Each has its procurement framework; procurement procedures and payments release requirements and processing time. This is inevitably reflected in contractors' bids pricing. It was found that contractors are quoting higher prices to the MOE comparing to what quoted to SFD and PWP. Taking into accounts the increase in quantities because of the design approach, and pricing different risks, the contractors quoted prices to MOE, PWP, and SFD that are 50%, 30%, and 25% higher than the actual price, respectively.

Can we get much better prices that reflect actual cost of materials and direct cost related to any contract? The data analysis shows that there is a high competition and a contractor would be very happy to receive a contract award, and would be happier if he can accomplish work as soon as he can in order to get payments.

If any improvement to be done it should be from the implementing agencies side. Good engineers should be contracted to produce school designs that are safe, functional, economic, and with minimal discrepancies. Choudhry (2017) attempted to identify the major causes of discrepancies in building construction. The results of the analysis indicate that the provision of incomplete data to designers, lack of interest by approving authorities to carefully check the design, and owner-proposed changes due to financial problems are the top three causes of discrepancies.

From the other side, more transparent and shorter cycle procurement procedure should be in place. Oyeyipo et al. (2016) conducted a study to evaluate the factors that affect contractors' decisions to bid for a project and to evaluate the importance of the identified factors to decision makers. The results indicate that the financial capability of clients, availability of capital and availability of material are the most important factors that contractors consider when making a bid/no bid decision.

In addition, contractors should be trained technically, and on procurement procedures so that be aware about their duties and rights. Site supervisors are a nightmare to contractors. Agencies should be selective, should train site engineers to play the right role of problem solvers rather than fishing mistakes, and create problems to both contractor and client.

Accommodating out-of-school children is a multi-dimensional issue, and is not only a matter of school building, but integrated educational policies and planning. Further studies on the subject matter will be of benefit to the findings of the current research work.

Acknowledgements

The researchers would like to thank the management and staff of the three agencies for providing access to their archives as well as our students who afforded time to collect the required data.

References

AL-kohlani M (2009). An investigation of the causes and extent of delay and cost overrun in school construction projects in Yemen. *M.Sc. thesis*, Bartlett School of Graduate Studies- University College London, UK.

AlMunifi A (1997). Lessons learned from Yemen earthquakes - engineering and environmental aspects. *29th General Assembly of IASPEI*. Thessaloniki, Greece.

AlMunifi A (2004). The vision of the Ministry of Education: Programs and policies. *The Pre-appraisal Workshop for the Preparation of the Basic Education Development Project*. Sana'a, Yemen.

Brown G (2013). Accelerating progress to 2015-Yemen. A Report Series to the UN Special Envoy for Global Education.

Choudhry R, Gabriel HF, Khan MK, Azhar S (2017). Causes of discrepancies between design and construction in the Pakistan construction industry. *Journal of Construction in Developing Countries*, 22(2), 1–18.

Döring C (2010). Cross-Sector and Multi-Institutional Assessments Study on School Construction Costs in Yemen. *The Proceedings of the 13th Architecture & Behaviour Colloquium*. Lausanne, Switzerland.

Dosumu OS (2018). Perceived effects of prevalent errors in contract documents on construction projects. *Construction Economics and Building*, 18(1), 1–26.

Fast Track Initiative (2004). Yemen experience with the fast track initiative. *Fast Track Initiative Partnership Meeting*. Brasilia.

GET German Education and Training (2008). School Construction Costs in Yemen. Sana'a, Yemen.

Government of Yemen (2018). Yemen Constitution. retrieved from http://www.yemen.gov.ye/. Jan 2019.

Günhan S, Arditi D, Doyle J (2007). Avoiding change orders in public school construction. *Journal of Professional Issues in Engineering Education and Practice,* 133(1), 67–73.

Khan Q, Chase S (2003). Yemen and the Millennium Development Goals. Working Paper Series. The World Bank.

Laryea S, Hughes W (2008). How contractors price risk in bids: Theory and practice, *Construction Management and Economics*, 26(9), 911–924.

Ministry of Education (2003). Analysis of the school construction 1996-2003. Sana'a, Yemen.

Ministry of Education (2004). Preparation of the school construction plans and policies.

Ministry of Education (2013). Yemen Education Sector Plan-Mid Term Results Framework 2013-2015.

National Information Center (2018). Law No. (23) for the year 2007 regarding tenders and auctions. https://www.yemen-nic.info/db/laws_ye/detail.php?ID=15594, Jan. 2019.

Ogawa K (2004). Achieving education for all in Yemen: Assessment and current status. *Journal of International Cooperation Studies*, 12, 2.

Oyeyipo O, Odusami KT, Ojelabi RA, Afolabi AO (2016). Factors affecting contractors' bidding decisions for construction projects in Nigeria. *Journal of Construction in Developing Countries,* 21(2), 21–35.

PWP (2018). Contracting procedures. Retrieved from www.pwpyemen.org/index.php/en/. Jan. 2019.

SFD (2018). Contracting procedures. The World Bank (2013). Report No: 72143-YE. Project Appraisal Document. Retrieved from www.sfd-yemen.org. Jan. 2019.

The World Bank (1999). Republic of Yemen-Education Sector Assistance Strategy. Human Development Sector.

The World Bank and the Republic of Yemen (2010). Education Status Report. Challenges and Opportunities. A joint publication of the International Bank of Reconstruction and Development.

The World Bank and Yemen Government (2005). Review of civil works components in four education projects. Mission Report.

UNICEF (2018). If not in school - The paths children cross in Yemen. Report.

Vincent M, Monkkonen P (2010). The impact of state regulations on the costs of public school construction. *Journal of Education Finance*, 35(4), 313–330.

Zaghloul R, Hartman F (2003). Construction contracts: The cost of mistrust. *International Journal of Project Management,* 21(6), 419–424.

Challenge Journal of Structural Mechanics

Research Article

Numerical modelling of heat transfer through protected composite structural members

Burak Kaan Cirpici *, Suleyman Nazif Orhan, Turkay Kotan

Department of Civil Engineering, Erzurum Technical University, 25050 Erzurum, Turkey

ABSTRACT

Among many various types of passive fire protection materials (i.e. plaster boards, sprayed materials and intumescent coatings) thin film intumescent coatings have become the preferable option owing to their good advantages such as flexibility, good appearance (aesthetics), light weight to the structure and fast application. Despite their popularity, there is also a lack of good understanding of fire behaviour. In general, experimental methods are used to push this knowledge with labour and high-energy consumption and extremely expensive processes. With the development of computer technology, numerical models to predict the heat transfer phenomena of intumescent coatings have been developed with time. In this work, the numerical model has been established to predict the heat transfer performance including material properties such as thermal conductivity and dry film thickness of intumescent coating. The developed numerical model has been divided into different layers to understand the sensitivity of steel temperature to the number of layers of intumescent coating and mesh sizes. The temperature-dependent thermal conductivity of intumescent coatings can be calculated based on inverse solution of the equation for calculating temperatures in protected steel according to the Eurocodes (EN 1993-1-2 and EN 1994-1-2). However, as the temperature distribution in the intumescent coatings is highly non-uniform, that Eurocode equation does not give accurate coating thermal conductivity-temperature relationship for use in numerical heat transfer modelling when the coating is divided into a number of layers, each having its characteristic thermal conductivity values. The comparison study of steel temperature under Standard (ISO 834) and Fast fire conditions against Eurocode analytical solution has also been made by assuming both constant thermal conductivity and variable thermal conductivity. The obtained results show close agreement with the Eurocode solution choosing a minimum certain mesh, number of layer and best-fitted thermal conductivity of the intumescent coating.

ARTICLE INFO

Article history:
Received 13 June 2019
Revised 19 July 2019
Accepted 6 August 2018

Keywords:
Intumescent coating
Heat transfer
Numerical model
Thermal conductivity
Composite floor
Steel beam

1. Introduction

Using steel with composite structural members such as slab is a major building construction type in commercial, residential and other buildings in worldwide. However, one big issue with steel as a building structural material is its poor behavior in fire due to rapid increase in temperature leading to sudden drop in strength. Moreover, high temperatures cause elongation and deformation in terms of decrease of the mechanical properties (Wang, 2002). Thus, fire protection is generally necessary to enable structural steel to survive under fire attack. Fire performance of various slim floors in fire with loading conditions has been studied by Alam et al. (2018). Besides, fire behavior of composite slab-beam systems has been investigated by Nguyen et al. (2015) by experimentally and numerically claiming that the experimental results provide only basic information on the membrane behavior in fire for the numerical models.

* *Corresponding author*. Tel.: 444-5-388 ; Fax: +90-442-230-0036 ; E-mail address: burak.cirpici@erzurum.edu.tr (B. K. Cirpici)
ISSN: 2149-8024 / DOI: https://doi.org/10.20528/cjsmec.2019.03.003

The parameters such as emissivity and the moisture content of the concrete effecting thermal performance of composite slabs have been given in the paper of Jiang et al. (2018) declaring that the moisture content with an increment of 1% leading to an increase on fire performance of the composite floor system. Among various types of fire protection materials, intumescent coatings are commonly used passive fire protection material owing to their ease and flexibility in application, good durability, aesthetic view and light weight. Intumescent coatings are specially formulated reactive paints designed to expand by a factor of between 5 to 100 times by releasing gases and forming a final char which acts as a thermal barrier (Horacek and Pieh, 2000; Mariappan, 2016; Zhang et al., 2012a, 2012b; Cirpici et al., 2016a, 2016b; Bourbigot et al., 2004; Di Blasi, 2004). Despite these advantages of intumescent coatings, the fire behavior of it has not been thoroughly understood because of the complexity of the expansion process, rate of temperature increase and the composition of the coatings.

Fire testing of intumescent coatings used in structural steel members is seen as necessary to cover different applications, but also an expensive process to the people like intumescent coating manufacturers and academicians. Therefore, the validation study in terms of steel temperature based on intumescent coating protected I-steel section has been performed with mesh sensitivity study firstly. Then, numerical heat transfer has been used to compute the temperatures in composite structural members in terms of steel beam, steel decking protected with intumescent coating and concrete under standard fire condition (ISO 834) specified by the International Standard Organization ((ISO) 2014) herein this study. The numerical simulations are accomplished by the Transient Thermal analysis module of ANSYS Workbench 18.1.

Nomenclature

λ_{st}	Thermal conductivity of steel
T_{st}	Steel temperature
C_{st}	Specific heat of steel
ρ_{st}	Density of steel
λ_p	Thermal conductivity of fire protection material
A_p/V	Section factor of the protected steel section
d_p	Fire protection material' thickness
c_p	Specific heat of fire protection material
ρ_p	Density of fire protection material
ΔT_f	Fire temperature differences respect to time

2. Validation Study based on I-Steel Section against Eurocode Solution

The validation study has been done based on comparing against Eurocode – EN 1993-1-2 (CEN, 2005a). Fig. 1 shows the 2-D intumescent coating protected steel system obtained from 3-D. Green line shows the intumescent coating applied to 4-side of the steel beam.

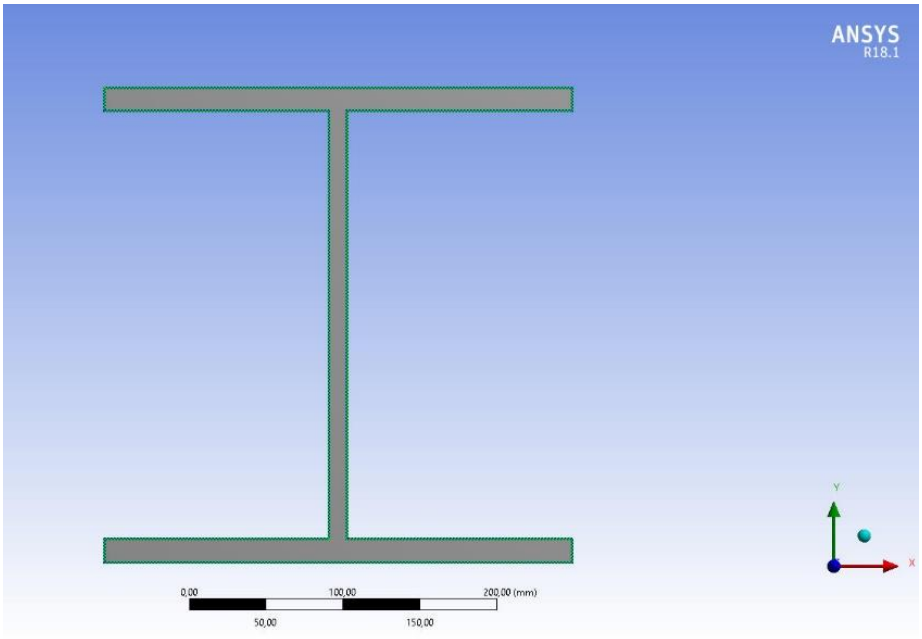

Fig. 1. ANSYS simulation 2-D view.

The intumescent coating used in this model has been assumed to be non-reactive fire protection material with no change in thickness. Therefore, the expansion process has not been considered in this validation. Although, this does not reflect the actual behavior of intumescent coatings, this is considered acceptable for the validation purpose.

2.1. Material thermal properties

The main required thermal properties for heat transfer analysis are specific heat, thermal conductivity, emissivity and density.

2.1.1. Steel properties

The thermal conductivity, specific heat and density of steel structural steel has been obtained from Eurocode 3 Part 1.2 (CEN, 2005a).

- The thermal conductivity of steel is:

If steel temperature T_{st} (K) is lower than 800°C;

$$\lambda_{st} = 54 - 3.33 \times 10^{-2}\, T_{st} \quad (1)$$

If steel temperature is higher than 800°C;

$$\lambda_{st} = 27.3 \quad (2)$$

where λ_{st} is the steel thermal conductivity (W/mK). Fig. 2 presents the thermal conductivity of steel-temperature relationship based on EN 1993-1-2.

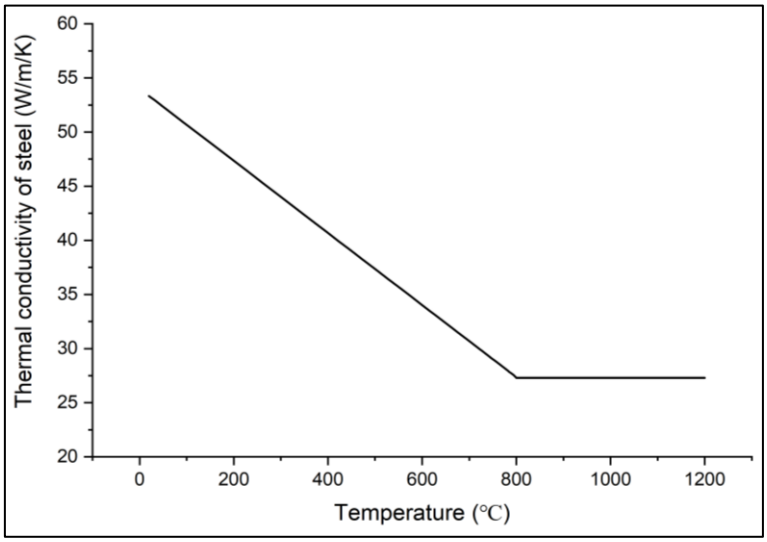

Fig. 2. Variation of thermal conductivity of steel with temperature (CEN, 2005a).

- The specific heat-temperature relation is:

If $20°C \leq T_{st} < 600°C$;

$$C_{st} = 425 + 7.73 \times 10^{-1} T_{st} - 1.69 \times 10^{-3} {T_{st}}^2 + 2.22 \times 10^{-6} {T_{st}}^3 \quad (3)$$

If $600°C \leq T_{st} < 735°C$;

$$C_{st} = 666 + \frac{13002}{738 - T_{st}} \quad (4)$$

If $735°C \leq T_{st} < 900°C$;

$$C_{st} = 545 + \frac{17820}{T_{st} - 731} \quad (5)$$

If $900°C \leq T_{st} < 1200°C$;

$$C_{st} = 650 \quad (6)$$

where C_{st} is the specific heat $\left(\frac{J}{kg} \cdot K\right)$ (Fig. 3).

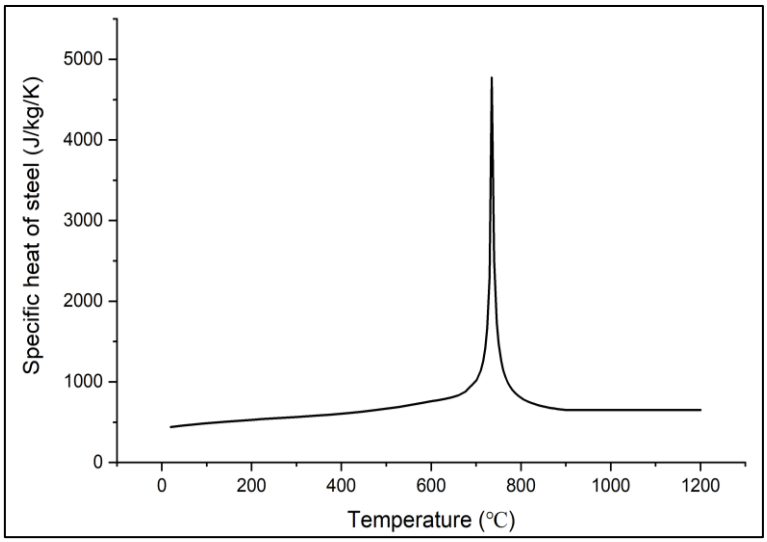

Fig. 3. Variation of specific heat of steel with temperature (CEN, 2005a).

Fig. 3 shows the specific heat of steel-temperature relationship based on EN 1993-1-2. The high values are around 735℃ as a result of change of microstructure of the steel. The density of structural steel used in the model is 7850 kg/m^3.

2.1.2. Intumescent coating thermal properties

As the thickness in the validation study is very small, the effect of its density and specific heat on the protected steel temperature is very little. Hence, the constant values according to Annex E of EN 13381-8:2013 (CEN, 2013) has been used. Those values are 1000 J/kg · K for the specific heat, and 100 kg/m^3 for the density respectively. However, the effective thermal conductivity has been obtained by Wang et al. (2013) based on their fire tests. This effective thermal conductivity-temperature relationship is shown in Fig. 4. In their model, fire has been exposed to the protected surfaces as it is also applicable herein author's study though. The considered convective heat transfer coefficient in the model is 25 W/m^{2}K (CEN, 2005a) and the resultant emissivity of the coating for the radiation has been taken as 0.92 (CEN, 2005a).

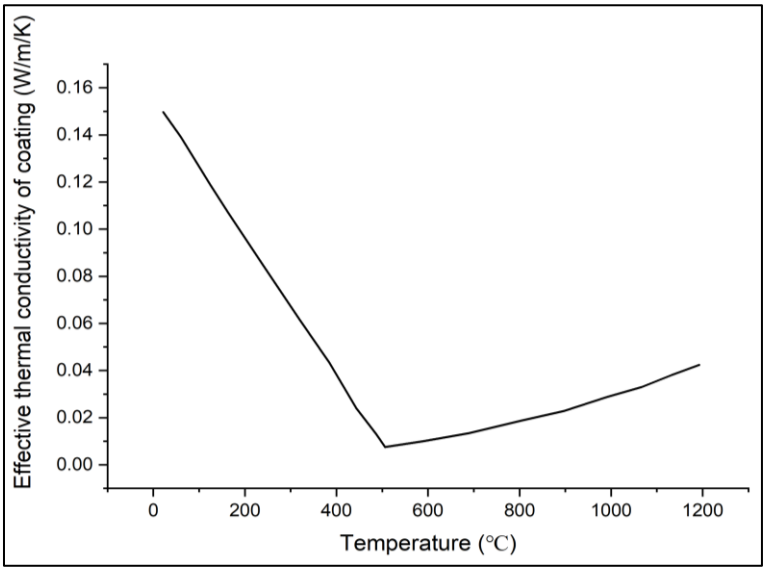

Fig. 4. Effective thermal conductivity-temperature curve (Wang et al., 2013).

2.2. Boundary conditions and relevant data for the validation

The relevant data for the simulation of intumescent coating protected I-section (305mm × 305mm × 97kg/m) has been tabulated in Table 1. This section has been exposed to the standard fire condition all around (4-side). The boundary conditions are shown in Fig. 5.

Table 1. Specimen details for comparison with Eurocode calculation.

Section	Dimensions (mm)			
305 × 305 × 97	B	D	T_f	T_w
	303	308	14.3	10.5
Protection thickness	1.0 mm			
Fire exposure	4-sided			
Steel properties $(\lambda_{st}, C_{st}, \rho_{st})$	EN 1993-1-2			
Protection properties (C_p, ρ_p)	EN 13381-8			
Protection thermal conductivity	Wang et al. (2013)'s study			

According to EN 1993-1-2, the temperature of a protected steel section is calculated using Eq. (7).

$$\Delta T_{st} = \frac{\lambda_p A_p/V}{d_p c_{st} \rho_{st}} \frac{T_f - T_{st}}{\left(1+\frac{\phi}{3}\right)} \Delta t - \left(e^{\phi/10} - 1\right)\Delta T_f$$

$$\text{with } \phi = \frac{c_p \rho_p}{c_{st} \rho_{st}} d_p \frac{A_p}{V} \tag{7}$$

where λ_p (W/mK) is the thermal conductivity of the fire protection material (intumescent coating shown in Fig. 4), A_p/V (m^{-1}) is the section factor of the protected steel section based on the diameter presented in Table 1, d_p (m) is the fire protection thickness, c_p (J/kg · K) and ρ_p (kg/m^3) are specific heat and density of the protection material given in Section 2.1.2, T_f (℃) and T_{st} (℃) is the exposed fire temperature (ISO) and steel temperature respectively, Δt (s) is the time interval in seconds.

The considered fire conditions (i.e. fire curves such as Standard (ISO) and Fast) as inputs for the developed models are shown in Fig. 6.

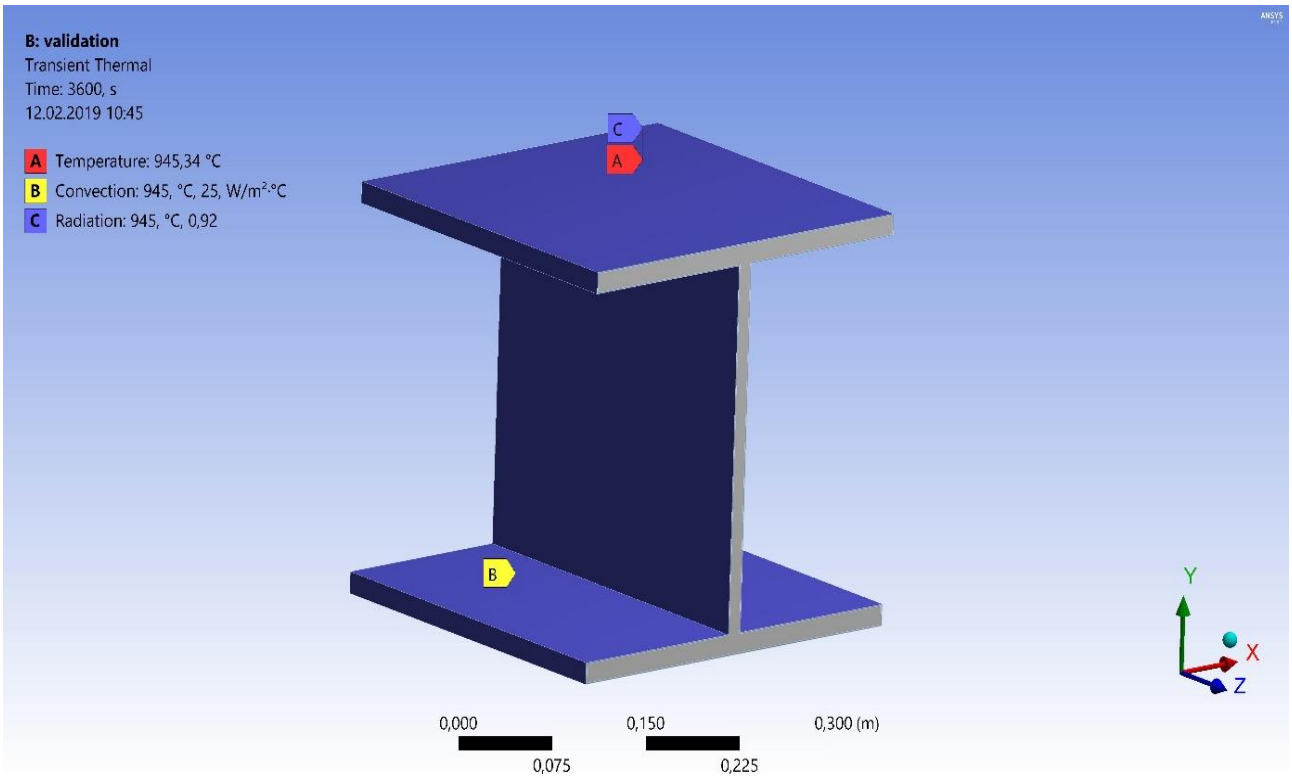

Fig. 5. Boundary conditions of the validation study.

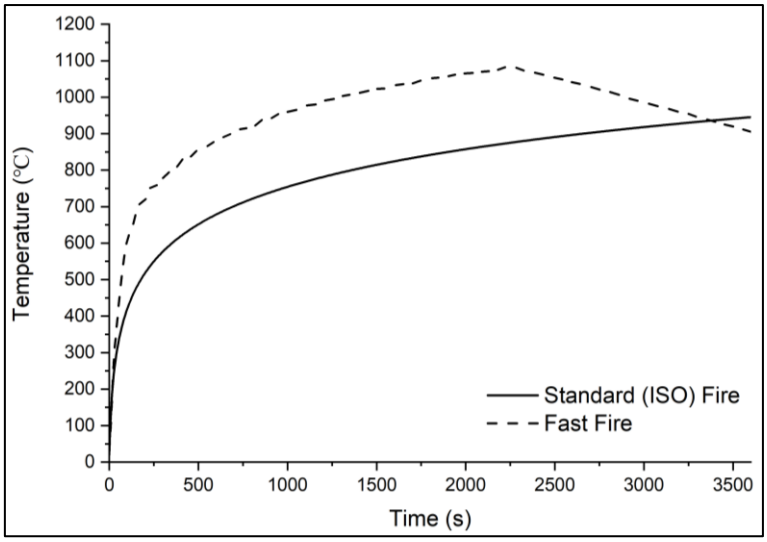

Fig. 6. Exposed fire conditions for the numerical models.

3. Results of Validation and Mesh Sensitivity Study

Fig. 7 compares the ANSYS simulation results and EN 1993-1-2 analytical solution results. As seen, very close results confirm the validity of the numerical model based on applied Standard (ISO) fire condition. Moreover, 3-D heat transfer simulations has been carried out using different mesh types and sizes. The steel temperature differences between author's results and Eurocode solution is significantly small up to 200°C since the intumescent coating is almost inert at around that temperature. However, the coating begins to be active afterwards with the increase in temperature. The differences are quite small with the range of 2-3% based on the mesh size of 2 mm and 5 mm. This also provides additional confidence in the authors' simulation model. It is concluded that the mesh sizes have a little effect on the predicted steel temperature. Tetrahedral elements have been used for meshing of coating as its section thickness is relatively thin. For the steel profile meshing, hexahedral elements have been preferred. Mesh structure has been presented in Fig. 8. From the mesh sensitivity study, mesh size of 5 mm are chosen for the intumescent coating as acceptable and will be used in the heat transfer simulations of composite slab with steel decking and steel beam.

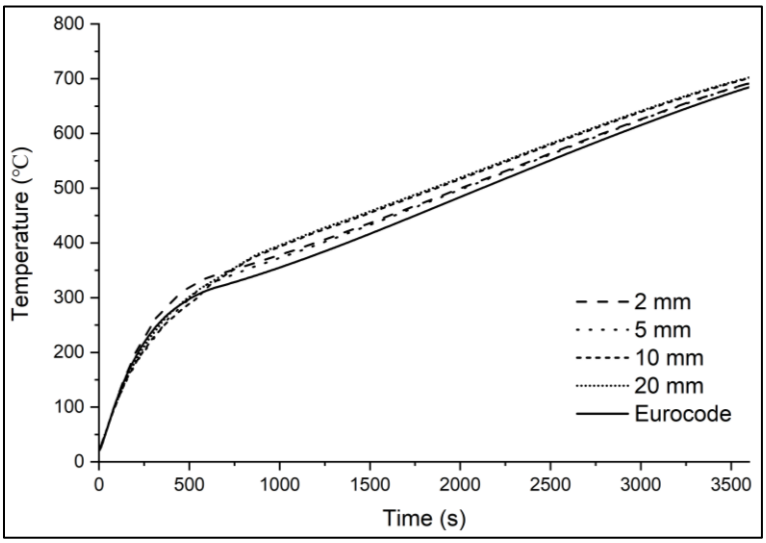

Fig. 7. Comparison of insulated steel temperatures predicted from ANSYS 3-D model and calculated according to EN 1993-1-2.

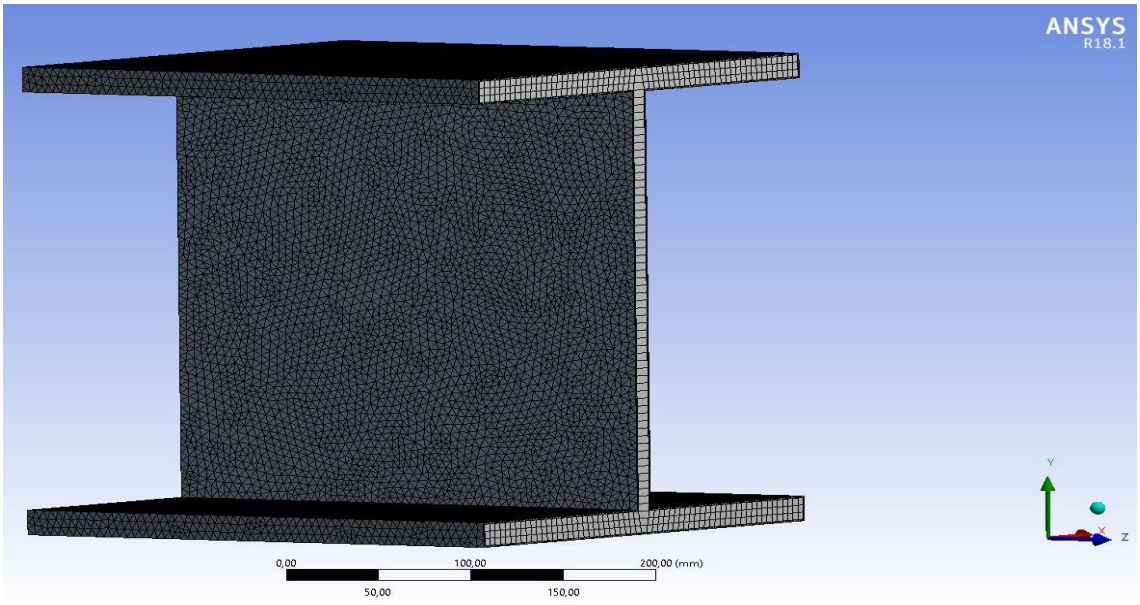

Fig. 8. Structure of the mesh for the validation study.

4. Temperature Distribution in Protected Composite Structural Member

After validating the developed 3-D model, a steel beam with a steel decking, both protected by intumescent coating supported a concrete slab on top in 3-D model has been developed to predict the steel temperatures for both decking and beam and concrete temperature after Standard fire (ISO 834) and Fast fire exposures to steel parts of the model.

For this purpose, two models has been proposed and developed. One of them is to apply intumescent coating to the steel parts with the same protection thickness (1 mm) with the validation model in one-layer. The other one is to apply the same coating by 4-layers. This study aims to understand how the layers have an influence on temperature distributions on proposed composite structural member. Moreover, it is also proposed to see the effect of fire exposure side (only to steel parts of the model) on the temperature distribution on both steel beam and decking and also concrete.

4.1. Model properties and setup

4.1.1. Steel beam and decking properties

In this study, in a typical composite steel-concrete flooring system whose geometric properties are shown in Fig. 9, two different model of which the same intumescent coating is applied in two different ways, were used. In the models; as floor structural beam, the section properties of the standard UC 305×305×97 steel profile and as composite decking, the section properties of a typical trapezoidal steel sheet produced for this purpose in Turkey (Ataçelik, 2019), have been considered here in this study. Two different composite floor system have been

modelled in two different ways considering that the intumescent coating as the fire protection material was applied to surfaces of the steel beam profile outside the cross-section and to only bottom surface of the trapezoidal steel sheet as a single layer with 1 mm thickness and successive four layers with 0.25 mm thickness. Since the intumescent coating is applied after the composite floor assembles, coating has not been applied to the parts of the trapezoidal steel deck where it is seated on the steel beam. In both composite floor models, as the same way, it was thought that the structural concrete parts of whom the deep section with 120 mm thickness, to be made of normal weight concrete. The length of composite floor models are 1 meter in transverse and longitudinal direction having one square meter unit surface area.

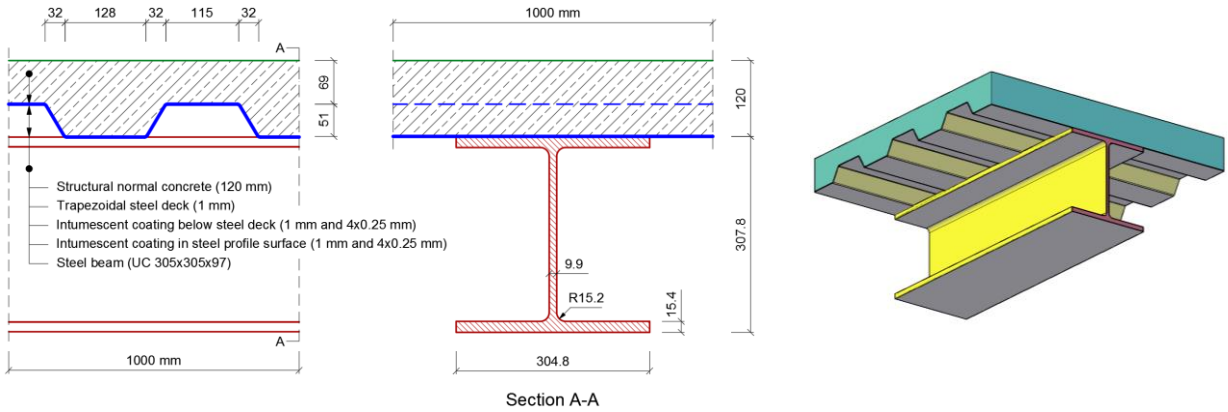

Fig. 9. Composite structural member properties.

4.1.2. Thermal properties of concrete

The variation of thermal conductivity of concrete with temperature depending on concrete weight (i.e. lightweight – LC, normal weight – NC) is illustrated in Fig. 10 (CEN, 2005b). Normal weight with lower limit values for the thermal conductivity of concrete has been considered in the developed ANSYS model.

Specific heat of normal weight concrete (NC) and lightweight concrete (LC) as a function of temperatures is given in Fig. 11 according to EN 1994-1-2 (CEN, 2005b). The change of specific heat of normal weight concrete respect to temperature input into the developed model as the considered concrete slab part of the composite structural member is normal weight concrete. The concrete density has been taken into account as 2400 kg/m^3. The unheated side (i.e. on the top of the slab) interacts with the environment through a coefficient of heat transfer by convection of 4 W/m^{2}K and a convection coefficient of 5 W/m^{2}K applied to the fire exposed face of the slab model (i.e. on the bottom of the slab) (Both et al., 2016).

4.1.3. Finite element model properties

Having the confidence of the validation model, composite structural member has been developed in the same way with the previous study adding the steel decking and concrete slab. The boundary conditions and the general mesh structure of the developed model has been shown in Figs. 12 and 13, respectively. Moreover, all contacts between the materials are modelled as bounded.

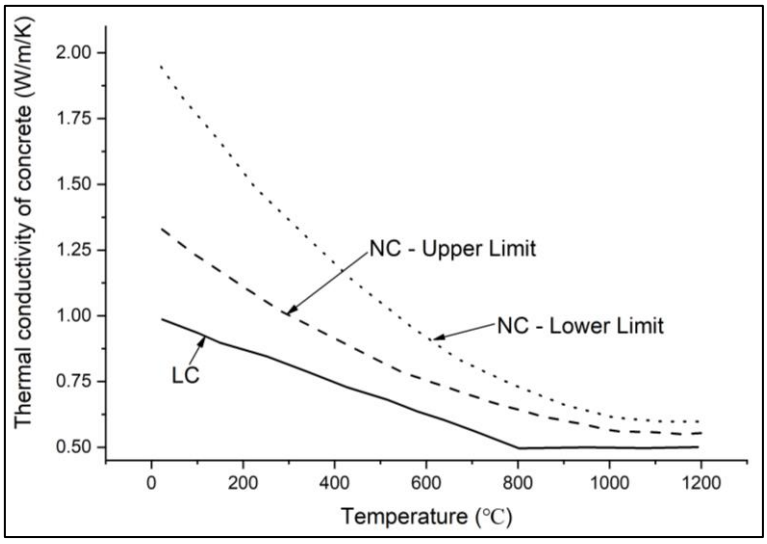

Fig. 10. The change of thermal conductivity of concrete respect to temperature.

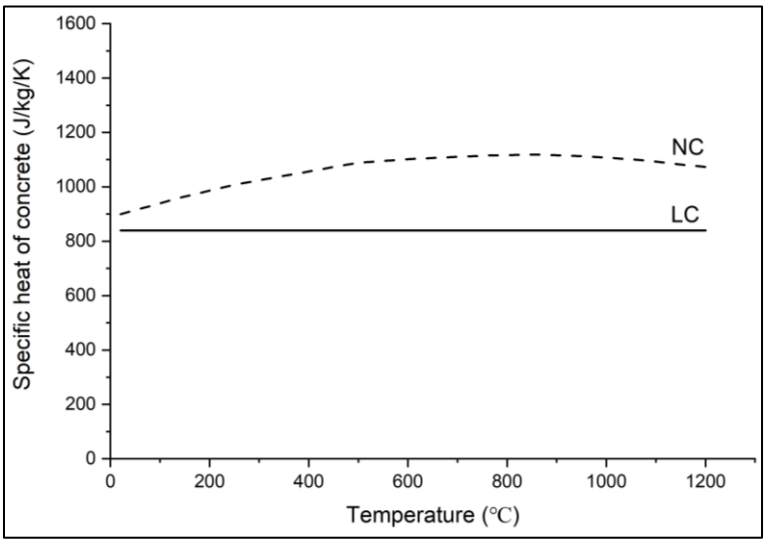

Fig. 11. Change of specific heat of normal weigh concrete (NC) and lightweight concrete (LC) with temperature.

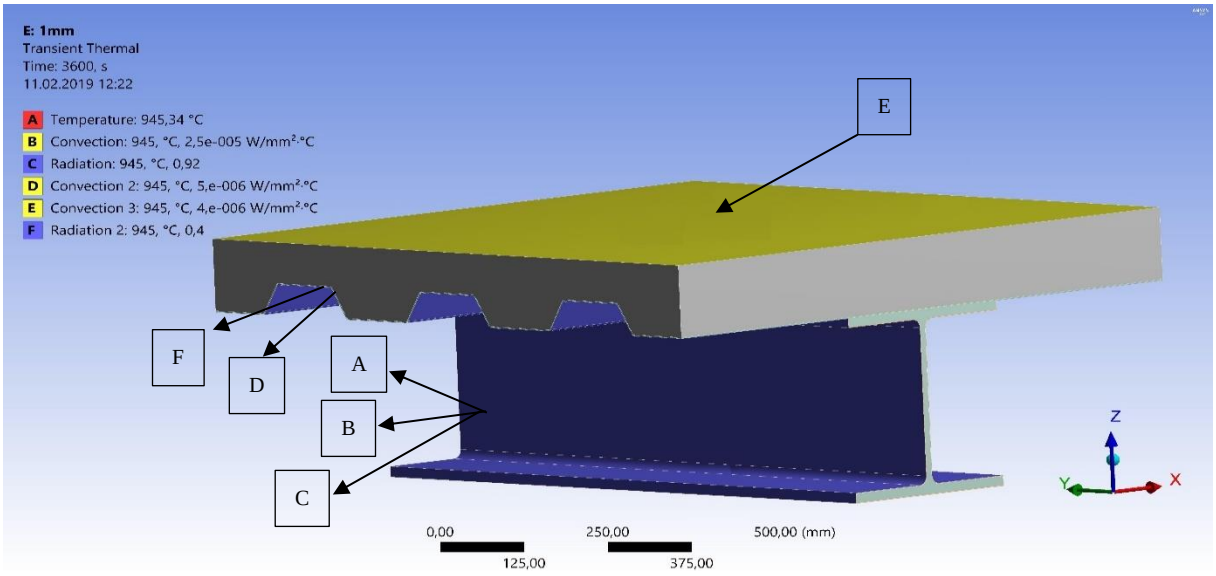

Fig. 12. Thermal boundary conditions of the composite structural member.

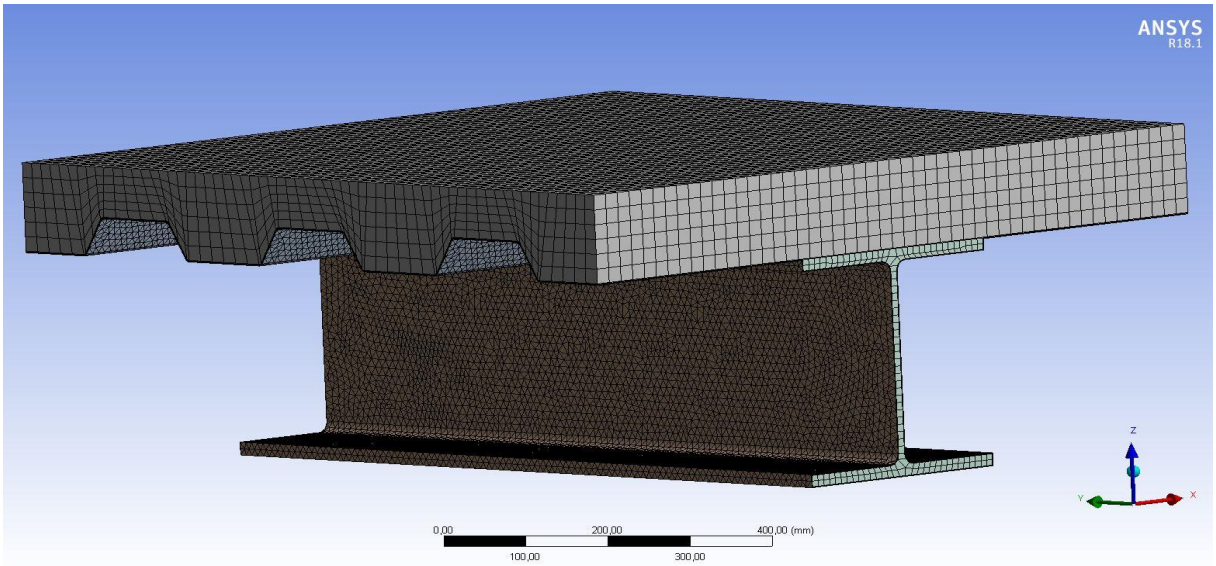

Fig. 13. Meshed models of composite structural member.

5. Results and Discussion

Fig. 14 shows the steel beam (UC 305×305×97) temperature-time relationship under the standard fire (ISO-834) exposure for an hour. The fire has been exposed to the surface where the coating has been applied on. As explained in Section 4.1.1, two different scenarios had been proposed, one layer of coating with 1 mm thickness and 4-layers of coating with 0.25 mm thickness individually. It is found that assigning number of layers to intumescent coating produced a bit less temperature results especially the coating has moved to be active around after 150°C. However, the differences between results of 1-layer and 4-layers has been decreasing when the intumescent coating turns into char after approximately 450°C. This was also obtained by Podolski (2017) where the author demonstrates the sensitivity of steel temperature to the different number of layers using 1, 2, 4, 6 and 12 layers. He concludes that using 4-layers is sufficient. The simulation results and this study also provides more information about which part of the composite structural floor system has been effected more under possible fire attack such as web of the beam, edges of the flanges of the beam, steel decking itself due to being thinness and also the parts of the floor system where the openings are (the openings between steel decking and steel beam). Fig. 15 shows this overall fire performance and behavior of the proposed composite structural member.

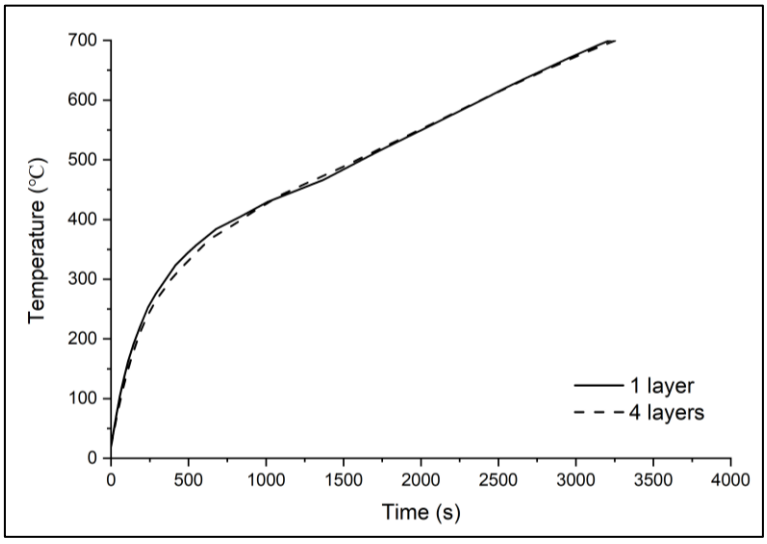

Fig. 14. Steel beam temperatures protected by intumescent coating with one-layer and 4-layers exposed to ISO 834 Standard fire.

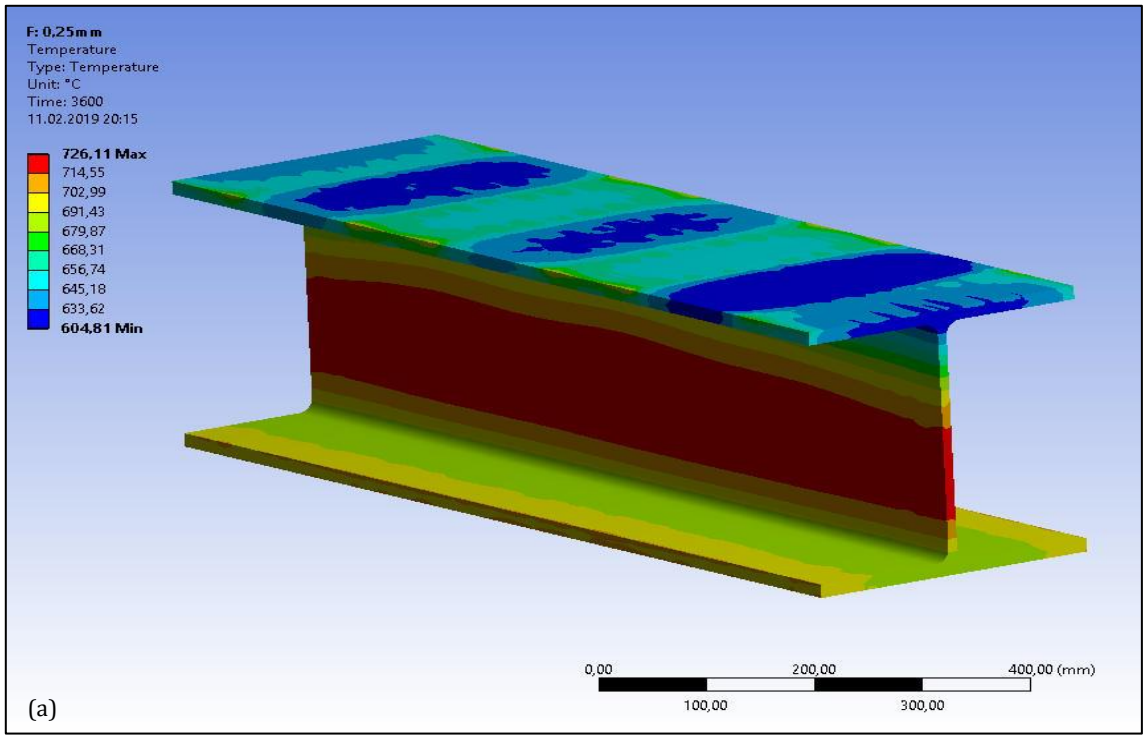

Fig. 15. (continued).

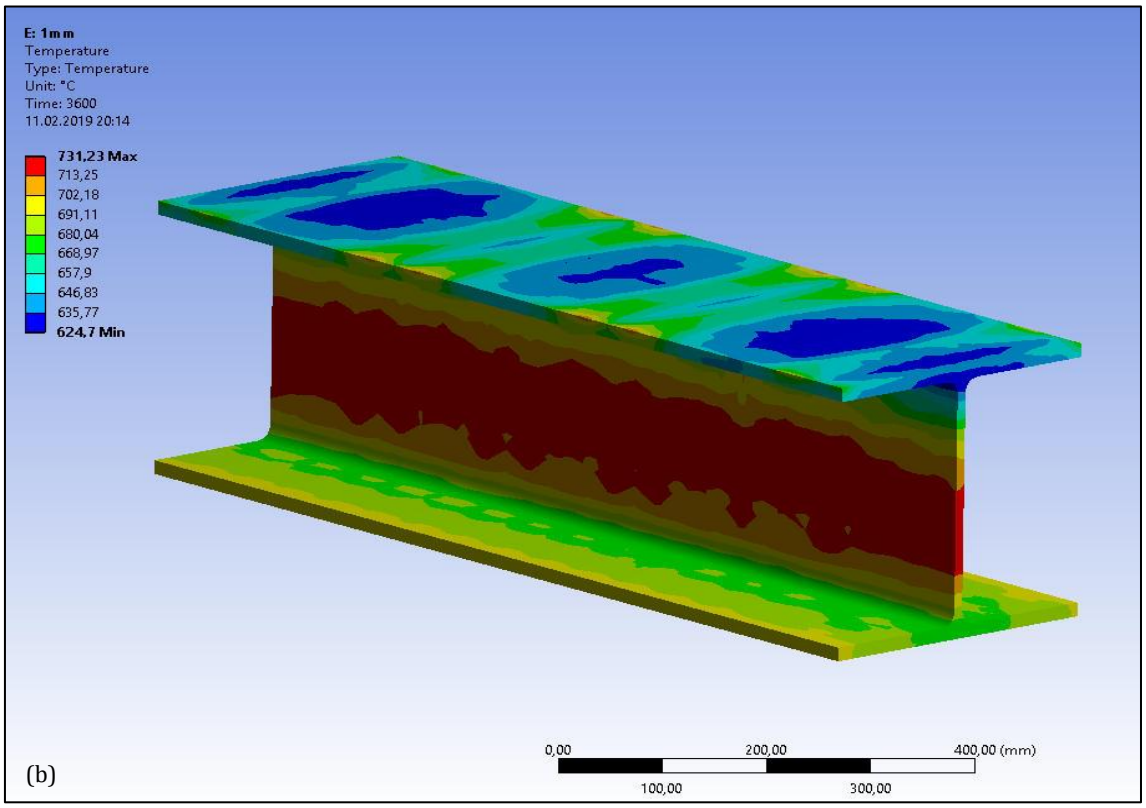

Fig. 15. The fire behaviour of the composite structural member under the exposure of Standard (ISO 834) fire: (a) applied 4-layers of coating each having 0.25 mm dry film thickness; (b) applied single layer having 1 mm dry film thickness.

Fig. 16 presents the steel beam temperature results of 1-layer and 4-layers of intumescent coating applied when it is exposed to Fast fire. Comparing to Standard (ISO) fire exposure, the difference between 1-layer and 4-layer results is a little bit more after approximately half one hour. At the end of the simulation, the temperature difference is just 25°C which can be acceptable when the heat transfer phenomena applies to layers. Beyond that, the identical behaviour and temperature results have been obtained for both 1-layer and 4-layers. Due to the nature of the Fast fire, the temperature increases rapidly contrast to Standard fire resulting in higher temperatures in the steel section almost 150°C differences. The overall fire performance and behaviour of steel beam after Fast fire exposure is shown in Fig. 17.

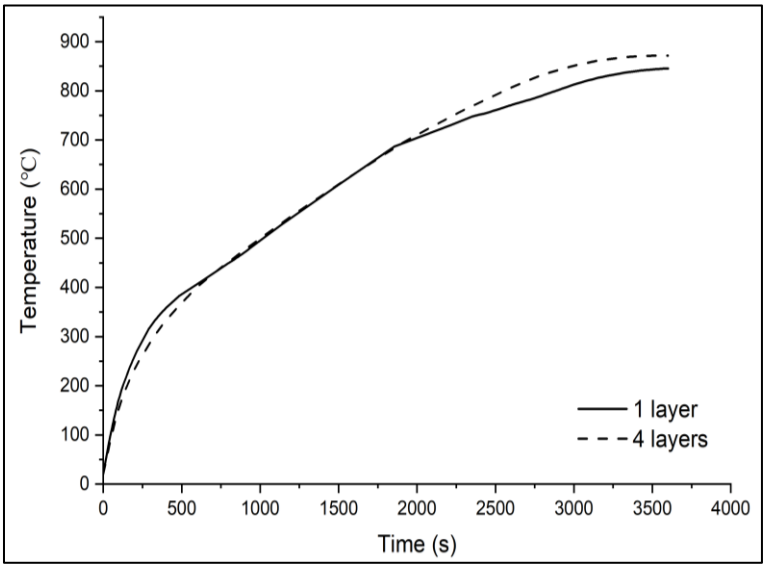

Fig. 16. Steel beam temperatures protected by intumescent coating with one-layer and 4-layers exposed to Fast fire.

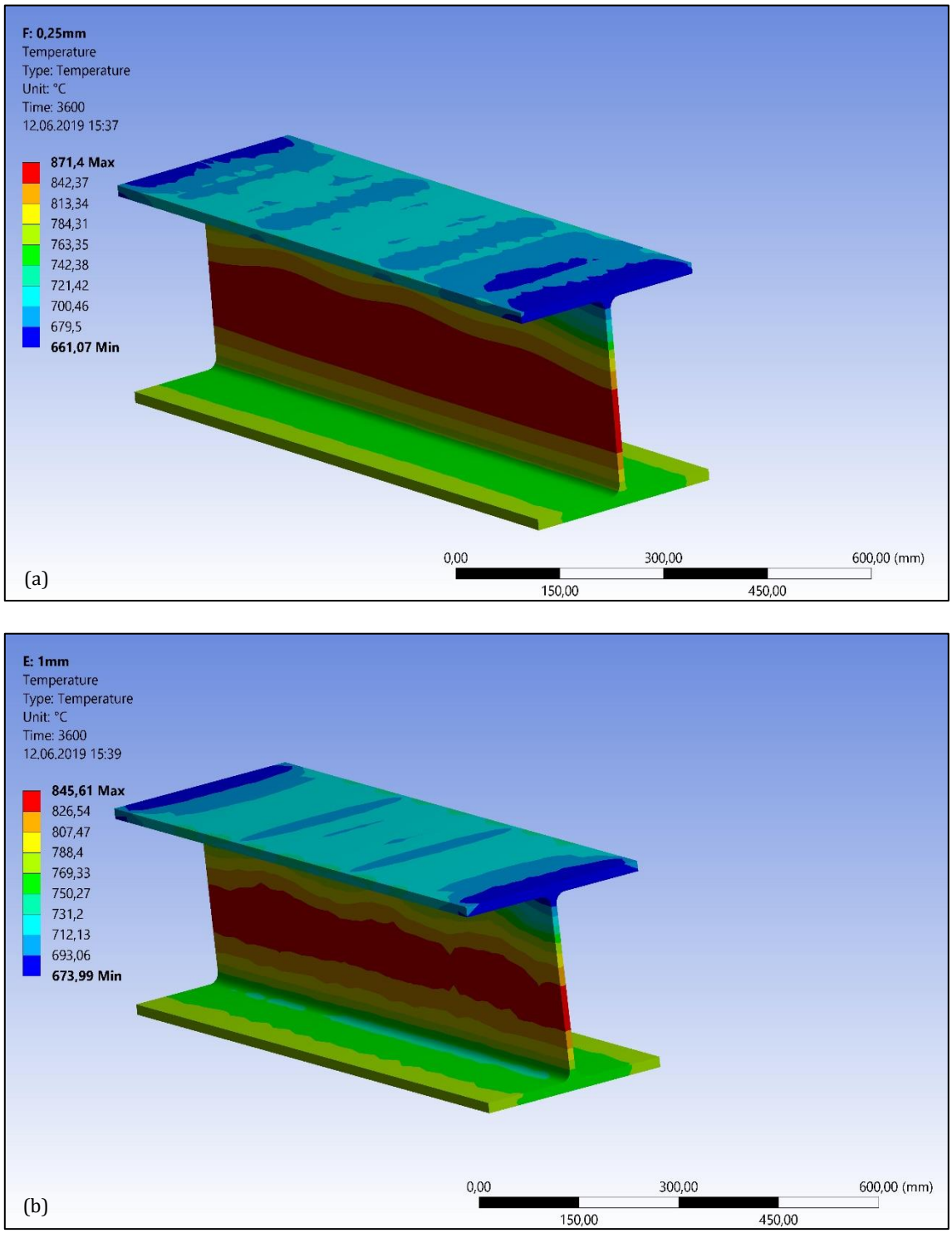

Fig. 17. The fire behaviour of the composite structural member under the exposure of Fast fire: (a) applied 4-layers of coating each having 0.25 mm dry film thickness; (b) applied single layer having 1 mm dry film thickness.

6. Conclusions

This study has presented the main features of a heat transfer simulation model using ANSYS and evidences to demonstrate that the simulation model is able to provide accurate results of intumescent coating protected steel temperature. Based on the results of the sensitivity and validation studies, the following numerical modelling parameters have been determined:

- A mesh size of 5 mm can be used with tetrahedral elements for the thinner parts and hexahedral elements for the thicker parts.
- The radiant and convective thermal boundary conditions obtained from Eurocode EN 1993-1-2 can safely be used to predict the protected steel temperature.
- The comparison of validation study is adequate.

For the study of composite structural member with steel beam, steel decking and concrete floor under the

exposure of both Standard and Fast fire, dividing the intumescent coating into layers gives more accurate results than considering single layer as it reflects the heat transfer behavior in a very good way. Moreover, the fire exposure side from steel parts to concrete results in fewer temperatures in concrete as it is expected because of good fire behavior and performance of concrete. In addition to this, this study also helps to understand which parts of the composite structural floor system influences more from a fire attack. Applying intumescent coating to steel parts including steel beam and decking provides a good fire protection performance to the whole structural system.

Publication Note

This research has previously been presented at International Civil Engineering and Architecture Conference (ICEARC'19) held in Trabzon, Turkey, April 17-20, 2019. Extended version of the research has been submitted to Challenge Journal of Structural Mechanics and has been peer-reviewed prior to the publication.

References

(ISO) I. O. f. S. (2014). ISO 834-11:2014 Fire resistance tests - Elements of building construction - Part 11: Specific requirements for the assessment of fire protection to structural steel elements.

Alam N, Nadjai A, Ali F, Nadjai W (2018). Structural response of unprotected and protected slim floors in fire. *Journal of Constructional Steel Research,* 142**,** 44-54.

Ataçelik (2019). *ADP92050 Tam Kesit Ozellikleri (ADP92050 Full Section Properties)* [Online]. Available: http://atacelik.net/PDF/P1_ATAPANEL.pdf [Accessed].

Both I, Wald F, Zaharia R (2016). Benchmark for numerical analysis of steel and composite floors exposed to fire using a general purpose FEM code. *Journal of Applied Engineering Science,* 14**,** 275-284.

Bourbigot S, Bras ML, Duquesne S, Rochery M (2004). Recent advances for intumescent polymers. *Macromolecular Materials and Engineering,* 289(6)**,** 499-511.

CEN (2005a). EN 1993-1-2: Eurocode 3. Design of Steel Structures. *Part 1.2: General Rules - Structural fire design.* BSI: London.

CEN (2005b). EN 1994-1-2:2005, Eurocode 4: Design of Composite Steel and Concrete Structures – Part 1-2: General Rules – Structural Fire Design. *Part 1-2: General Rules – Structural Fire Design.* BSI: London.

CEN (2013). EN 13381-8:2013 Test methods for determining the contribution to the fire resistance of structural members. *Part 8: Applied reactive protection to steel members.* BSI: London.

Cirpici BK, Wang YC, Rogers B (2016a). Assessment of the thermal conductivity of intumescent coatings in fire. *Fire Safety Journal,* 81**,** 74-84.

Cirpici BK, Wang YC, Rogers BD, Bourbigot S (2016b). A theoretical model for quantifying expansion of intumescent coating under different heating conditions. *Polymer Engineering & Science,* 56(7)**,** 798-809.

Di Blasi C (2004). Modeling the effects of high radiative heat fluxes on intumescent material decomposition. *Journal of Analytical and Applied Pyrolysis,* 71(2)**,** 721-737.

Horacek H, Pieh S (2000). The importance of intumescent systems for fire protection of plastic materials. *Polymer International,* 49(10)**,** 1106-1114.

Jiang J, Main JA, Weigand JM, Sadek FH (2018). Thermal performance of composite slabs with profiled steel decking exposed to fire effects. *Fire Safety Journal,* 95**,** 25-41.

Mariappan T (2016). Recent developments of intumescent fire protection coatings for structural steel: A review. *Journal of Fire Sciences*, 34(2)**,** 120-163.

Nguyen TT, Tan KH, Burgess IW (2015). Behaviour of composite slab-beam systems at elevated temperatures: Experimental and numerical investigation. *Engineering Structures,* 82**,** 199-213.

Podolski D (2017). Temperature Distribution in Intumescent Coating Protected Steel Sections. *M.Sc. thesis*, University of Manchester, Manchester, UK.

Wang LL, Wang YC, Yuan JF, Li GQ (2013). Thermal conductivity of intumescent coating char after accelerated aging. *Fire and Materials*, 37(6)**,** 440-456.

Wang YC (2002). Steel and Composite Structures - Behaviour and Design for Fire Safety. Spon Press, London.

Zhang Y, Wang YC, Bailey CG, Taylor AP (2012a). Global modelling of fire protection performance of an intumescent coating under different furnace fire conditions. *Journal of Fire Sciences,* 31(1)**,** 51-72.

Zhang Y, Wang YC, Bailey CG, Taylor AP (2012b). Global modelling of fire protection performance of intumescent coating under different cone calorimeter heating conditions. *Fire Safety Journal,* 50**,** 51-62.

Challenge Journal of Structural Mechanics

Research Article

Parametric investigation for discrete optimal design of a cantilever retaining wall

Esra Uray [a,*], Serdar Çarbaş [b], İbrahim Hakkı Erkan [c], Özcan Tan [c]

[a] *Department of Civil Engineering, KTO Karatay University, 42020 Konya, Turkey*
[b] *Department of Civil Engineering, Karamanoğlu Mehmetbey University, 70100 Karaman, Turkey*
[c] *Department of Civil Engineering, Konya Technical University, 42250 Konya, Turkey*

ABSTRACT

In this paper, discrete design optimization of a cantilever retaining wall has been submitted associated with a detailed parametric study of the wall. In optimal design, the minimum wall weight is treated as the objective function. Through design algorithm, the optimal design variables (base width, toe width, thickness of base slab and angle of front face) yielded minimum structural weight of the wall and satisfied stability conditions have been determined for different soil parameter values. At the end, a detail parametric study searching the effect of change of soil parameters on the retaining wall design has been conducted with 120 optimized wall designs for different values; eight values of the angle of internal friction, three values of the unit volume weight and five values of wall heights. The obtained results from optimization analyses indicate that change of the angle of internal friction more effective than change of the unit volume weight on the optimal wall weight. Economic wall design with optimization analysis is achieved in a shorter time than the traditional method.

ARTICLE INFO

Article history:
Received 16 July 2019
Revised 27 August 2019
Accepted 6 September 2019

Keywords:
Cantilever retaining wall
Structural optimization
Metaheuristics optimization method
Discrete design optimization

1. Introduction

In geotechnical engineering, the retaining walls are employed to resist lateral soil load in case of constructing works like an excavation, slopes, railway or highway as lateral support. In conventional design of a retaining wall, stability conditions like sliding and overturning are checked by using selected wall dimensions, firstly. If selected wall dimensions do not ensure stability conditions, this trial and error process is continued, till satisfying stability conditions. Even though safe wall dimensions have been obtained in plenty of time, it is not certain that obtained wall design is the most economic among all possible solutions. On the other hand, conditions of worksite like ground water level, soil height to be supported laterally or intended use of structure and soil properties such as bearing capacity or behavior of settlement under loads of soil should be considered in case of design. Existing of all mentioned situations in wall design with reasonable cost make this design a challenging engineering problem with many unknowns. Optimization methods have been commonly employed to obtain optimal solution of these kind of complex engineering problems by Rhomberg and Street (1981) and Keskar and Adidam (1989).

In real world problems, the existence of some cases like the sophisticated characteristics of problems with many unknowns, an infinite solution space, or the numerous iterations have given metaheuristic optimization methods prominence. The metaheuristic optimization algorithms, which are quite popular in recent years, have been used effectively in solving such problems over the last two decades. Popularity of metaheuristics that mimics the natural phenomenon is based on being simple, compatible and effective. While, preliminary information is required to solve the problem normally, such advantages eliminate this necessity even in the case of a broad array of optimization problems. Metaheuristics have been commonly utilized for solving engineering problems with multiple variables in case of deterministic

* *Corresponding author*. Tel.: ++90-332-221-7251 ; Fax: +90-332-202-0044 ; E-mail address: esra.uray@karatay.edu.tr (E. Uray)
ISSN: 2149-8024 / DOI: https://doi.org/10.20528/cjsmec.2019.03.004

and conventional methods are insufficient to obtain solutions. By using these algorithms, such as the genetic algorithms (GA) by Chau and Albermani (2003), the simulated annealing algorithm (SA) by Ceranic et al. (2003), the particle swarm optimization (PSO) by Khajehzadeh et al. (2010), the big bang-big crunch algorithm (BB-BC) by Camp and Akın (2012), the firefly algorithm (FA) by Sheikholeslami et al. (2014), the charged system search algorithm (CSS) by Talatahari and Sheikholeslami (2014), the gravitational search algorithm (GSA) by Khajehzadeh and Eslami (2012) and the teaching learning-based optimization (TLBO) by Temür and Bekdaş (2016), have all been investigated in the optimal design of a retaining wall. For this purpose, the particle swarm optimization (PSO), firefly algorithm (FA) and cuckoo search (CS) algorithm, known as swarm intelligence, have been employed to compare the results of studies by Gandomi et al. (2015). Parameters as the total wall weight, the angle of internal friction and the unit volume weight play an important role in retaining wall design which must satisfy stability conditions and must be economical. Effect of those parameters on the optimal design of a wall has been investigated as a parametric study and results have been presented by Yepes et al. (2008) and Molina-Moreno et al. (2017).

In this study, harmony search algorithm (HSA), which is a relatively contemporary metaheuristic optimization method, has been employed with the aim of investigating the safe and economic wall design. The algorithm firstly proposed by Geem et al. (2001) is based on harmony of sounds coming from each musical instrument in an orchestra. The HSA is more favorable than other metaheuristic algorithms and makes it possible to get results in less time without trapping local optimals. In addition, it can be used both continues and discrete variables and is easy to use in optimization process. It is proved that the HSA is a steady and fertile technique, which is impressively performed to derive solutions for a broad array of real-sized optimum design problems (Lee et al., 2005). In the literature, prosperous studies have been conducted like in structural optimization by Saka and Çarbaş (2009) and Bekdaş and Niğdeli (2016), in hydraulics by Ayvaz and Elçi (2013), in vehicle routing by Geem et al. (2005) and in geotechnical engineering by Cheng et al. (2011). Besides, improved, modified and hybrid version of HS algorithm which increase robustness and convergence of algorithm has been proposed with better optimum results of benchmark problem. New versions of HSA have been employed for optimum design of foundation presented by Khajehzadeh et al. (2011) and assignation of critical surface of slope presented by Cheng (2009) and Fattahi (2015). HSA is utilized successfully for optimization of reinforced cantilever retaining walls in realized studies by Akın and Saka (2010) and Uray et al. (2015).

The weight of the cantilever retaining wall has been optimized by using the HSA in this paper. In the discrete optimal design procedure, the wall dimensions selected from pre-dimension sets must satisfy the stability conditions and must be cost efficient. For this reason, numerous iterations and computational time are required to obtain the optimal dimensions. In the optimization problem, the dimensions of the retaining wall are taken as discrete design variables along with the effect of the soil properties of the backfill. To obtain the safe design which satisfy stability conditions, safety factors of sliding and overturning have been taken into consideration as design constraints with geometric restrictions. Finally, the optimal dimensions of the wall that are given minimum wall weight and satisfy the constraints are obtained. Furthermore, a detail parametric study has been performed for different design parameters to investigate effect of parameter change on optimal wall design. In the design optimization process of a cantilever retaining wall, only the weight of concrete has been taken into consideration.

2. Materials and Method

2.1. Formulation of the optimization problem

The cantilever retaining wall model is acquired with reference to the provisions of Building Code Requirements for Structural Concrete (ACI 318-08, 2008) and LRFD Bridge Design Specifications (AASHTO, 2010) so that it satisfies the structural stability. The general mathematical formulation of optimal retaining wall design is given below by Eq. (1).

Minimum value of objective function: $f_{min}(x) = W_{wall}$

Constraints to be employed:

$$g_i(x)=g_1(x), g_2(x), g_3(x), g_4(x) \leq 0 \ (x_l \leq x_i \leq x_u) \quad (1)$$

where x_l and x_u present lower and upper borders of design variables, whose number is equal to i.

In the optimal design problem, the base width (X_1), the toe width (X_2), thickness of base slab (X_3) and the angle of front face (X_4) are treated as discrete design variables tabulated in Fig. 1, and also the acting loads are shown in the same figure. Due to the design variables correspond to dimensions of the cantilever retaining wall, these variables and their intervals has been selected as discrete to achieve integer wall dimensions.

The lower and upper borders of the variables of optimal design, designated in Table 1, are determined by taking into consideration of the design provisions. In optimum design of the wall, design variables have been determined interrelated each other to obtain reasonable dimensions except the angle of front face (X_4). For instance, the base width (X_1) depend on the wall height (H), which changes range between $0.30H$ and $1.0H$, similar to other design variables.

The bottom thickness of the stem, b_b, is given by Eq. (2).

$$b_b = (H - X_3)\, X_4 + b \quad (2)$$

As the optimal design weight is more significant than the optimal design cost (Temur and Bekdaş, 2016), the goal function has retrieved as the total weight of the cantilever retaining wall. The weight W_1, W_2 and W_3, of Eq. (3) are explained with regard to design variables as shown in Eqs. (4) to (6). The soil weight of backfill (W_4), the active soil pressure (P_a), the passive soil pressure (P_p), the active soil pressure coefficient (K_a) and the passive soil pressure coefficient (K_p) are given in Eqs. (7) to (11) respectively.

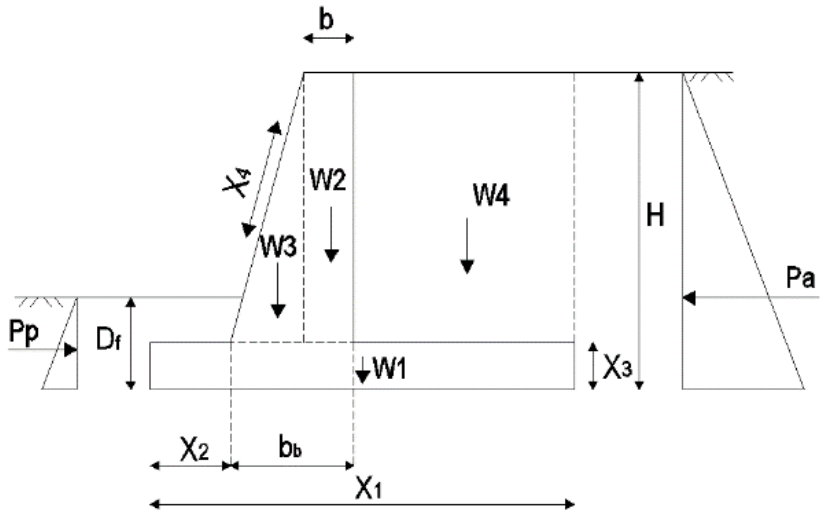

Fig. 1. Cantilever retaining wall and design variables.

Table 1. Design variables and limit bounds.

Design variables	Lower bound	Upper bound	Interval
X_1: Base width	$0.30H$	$1.0H$	$0.02H$
X_2: Toe width	$0.15X_1$	$0.55X_1$	$0.02X_1$
X_3: Thickness of base slab	$0.06H$	$0.16H$	$0.005H$
X_4: Angle of front face	%2	%7	%0.5

$$W_{wall} = W_1 + W_2 + W_3 \quad (3)$$

$$W_1 = X_1 X_3 \gamma_c \quad (4)$$

$$W_2 = b\,(H - X_3)\,\gamma_c \quad (5)$$

$$W_3 = (b_b - b)(H - X_3)\,0.5\,\gamma_c \quad (6)$$

$$W_4 = (X_1 - X_2 - b_b)(H - X_3)\,\gamma_s \quad (7)$$

$$P_a = 0.5H^2 \gamma_s K_a \quad (8)$$

$$P_p = 0.5{D_f}^2 \gamma_s K_p \quad (9)$$

$$K_a = tan^2(45 - \emptyset/2) \quad (10)$$

$$K_p = tan^2(45 + \emptyset/2) \quad (11)$$

The design constraints in the formulation of design optimization problem are so-called safety factors of sliding and overturning and the geometric constraints of the wall. The factor of safety against sliding and overturning is taken as 1.3 and the constraints of normalized mathematical expressions are given by the Eqs. (12) and (13), respectively.

$$g_1(x) = 1.3 - \frac{F_{resistant}}{F_{sliding}} \leq 0 \quad (12)$$

$$g_2(x) = 1.3 - \frac{M_{resistant}}{M_{overturning}} \leq 0 \quad (13)$$

Here, $F_{\text{resistant}}$, in Eq. (14), is a resistant force against to sliding of the wall and F_{sliding}, in Eq. (15), is a shift force, which causes sliding the wall. Similarly, $M_{\text{resistant}}$, in Eq. (16), is a resistant moment against to overturning of the wall and $M_{\text{overturning}}$, in Eq. (17), is an overturning moment which causes overturning the wall. To satisfy safety factor of sliding and overturning stability of the wall, $g_1(x)$ and $g_2(x)$ must be equal or greater than 1.3. In addition, the normalized mathematical expressions of the geometric constraints of the wall, $g_3(x)$ and $g_4(x)$, are given by the Eqs. (18) and (19).

$$F_{resistant} = (W_1 + W_2 + W_3 + W_4)\,tan\,\delta + P_P \quad (14)$$

$$F_{sliding} = P_a \quad (15)$$

$$M_{resistant} = W_1\left(\frac{X_1}{2}\right) + W_2\left(b_b - \frac{b}{2} + X_2\right) + W_3\left(\frac{2}{3}(b - b_b) + X_2\right) + W_4\left(\frac{X_1 + X_2 + b_b}{2}\right) + P_p\,\frac{D_f}{3} \quad (16)$$

$$M_{overturning} = P_a\left(\frac{H}{3}\right) \quad (17)$$

$$g_3(x) = \frac{b}{b_b} - 1 \leq 0 \quad (18)$$

$$g_4(x) = \frac{X_2 + b_b}{X_1} - 1 \leq 0 \quad (19)$$

In Table 2, design parameters used in the optimization analyses are given. In design of the cantilever retaining wall, the wall height has an important role for calculation of the acting loads to the wall depends on directly wall height. Other important parameters are the soil properties of backfill, the unit volume weight and the angle of internal friction. Coefficient of friction (δ) between wall and soil is taken as equal to the angle of internal friction during optimization process.

Table 2. Design parameters.

Parameter	Value
H: Wall height (m)	4-5-6-7-8
γ_s: Unit volume weight (kN/m^3)	16-18-20
Ø: Angle of internal friction (°)	20-22-24-26-30-35-40-45

2.2. Harmony search algorithm

Heuristic methods are algorithms that inspired from solutions produced by nature for difficult problems. HSA (Geem, 2001) which is a relatively novel metaheuristic optimization algorithm is related to find the best tonality in music process similar to producing the best solutions for complex optimization problems. In the optimal design of a cantilever retaining wall, the design variable values are decided by utilizing a design pool comprising the discrete variables as depicted in Table 1. The HSA has been employed in order to solve the design problem with inequality constraints containing those discrete design variable values and to reach the optimal objective function productively.

Steps of harmony search algorithm whose flowchart is demonstrated in Fig. 2 are as follows:

Step 1: Determination of algorithm parameters (*HMS*, *HMCR* and *PAR*), maximum iteration number and pool of design parameters;

Step 2: Initialization of harmony memory matrix (*HM*);

Step 3: Improvisation of new harmony based on three rules (NCHV);

Step 4: Updating of harmony memory matrix;

Step 5: Checking of termination criterion.

Algorithm parameters as harmony memory size (*HMS*), the harmony memory considering rate (*HMCR*), the pitch adjusting rate (*PAR*) and the maximum number of iterations are selected and design pool is formed by using design variables of optimization problem. Harmony memory matrix (*HM*) which is given by Eq. (20) is formed randomly by using design variables from design pool. In this equation, while the row number of *HM* corresponds to *HMS*, number of design variables (*N*) are equal to the columns number of matrix. For values of x_{ij} given by Eq. (20), values of *i* and *j* are respectively from 1 to *HMS* and from 1 to *N*. For current value of *j*th (*j*=1,…,*N*) are selected randomly design pool in *i*th possible solution and this process is repeated for each rows (*i*=1,…..,*HMS*). And then values of objective function are calculated for each row of *HM* which is a potential solution and sorted ascending or descending order according to aim of minimization or maximization objective function.

$$HM = \begin{bmatrix} x_{1,1} & x_{2,1} & \cdots & \cdots & x_{N-1,1} & x_{N,1} \\ x_{1,2} & x_{2,2} & \cdots & \cdots & x_{N-1,2} & x_{N,2} \\ \cdots & \cdots & \cdots & \cdots & \cdots & \cdots \\ \cdots & \cdots & \cdots & \cdots & \cdots & \cdots \\ x_{1,HMS-1} & x_{2,HMS-1} & \cdots & \cdots & x_{N-1,HMS-1} & x_{N,HMS-1} \\ x_{1,HMS} & x_{2,HMS-1} & \cdots & \cdots & x_{N-1,HMS} & x_{x_{N,HMS}} \end{bmatrix} \quad (20)$$

In improvisation of a new harmony memory matrix, it is checked whether or not there is better solution. For this process, possibilities of *HMCR*, *PAR* and (1-*HMCR*) are taken into consideration. If randomly selected number between 0 and 1 is smaller than *HMCR*, the index number of current design variable is changed with possibility of *HMCR* selected value from *HM*. If it is not, the index number is selected randomly with the possibility of (1-*HMCR*) from design pool. Revision of pitch adjusting rate (*PAR*) is just applied for changed values with *HMCR* possibility. This improvisation is repeated for all design variables (*j*=1,…,*N*) and then new solution harmony is obtained.

After improvisation of a new harmony, it is checked whether it should be good solution or not according to value of calculated objective function. If the new value of objective function is better than the worst value of objective function, new solution is saved in *HM* and the worst solution is deleted from *HM*. This process is continued until current iteration number reaches to maximum iteration number.

3. Analysis and Results

In optimization analyses, optimization algorithm is coded by using MATLAB software and 120 retaining wall designs in cohesionless soil have been carried out for different values of the wall height (*H*=4, 5, 6, 7, 8 m), the unit volume weight (γ_s=16, 18, 20 kN/m^3), the angle of internal friction (Ø=20, 22, 24, 26, 30, 35, 40, 45°). Firstly, value of *H*, γ_s, Ø and *HMS*, *HMCR*, *PAR* and maximum iteration number have been identified for each design. The discrete design variables (X_1, X_2, X_3 and X_4) given in Fig. 1 have been employed and design pool is formed by considering their upper and lower borders given Table 1. In the solution of the optimization problem, a new solution is obtained by using values of the discrete design variables selected from the design pool randomly. According to a new solution, which satisfies the constraints given by the Eqs. (12), (13), (18) and (19), the minimum goal function given by Eq. (3) value and the optimal wall dimensions have been calculated. The top thickness of the stem is taken as *b*=0.25 m and the depth of the foundation is taken as D_f=1.5 m for all optimization analyses.

In this study, the parameters of the HSA are chosen as *HMS*=20, *HMCR*=0.95 and *PAR*=0.15. The values of those parameters are allocated at the beginning and they stay unchanged during the optimization process. The most suitable range of parameter values are included in the studies of Lee et al. (2005). According to separate optimization problems from various fields, it is asserted that the values of the parameters are related with search space dimension. That's why the impact of the selected parameters is examined in each design example in current study. Thus, the proposed HSA is executed several times for each design problem by taking into account the various set of parameters. Afterward, carrying out the sufficient amount of run for sensitivity of the predetermined parameters, abovementioned HSA parameters are decided to utilize for having the least wall weight. To ensure the optimal values, which are obtained with the algorithm, the numerous iterations have been performed and the optimal values have been found with 5,000 iterations. In process of the optimal design, it has been observed that the optimal result remains the same after 5,000 iterations.

In the sequent sections, the optimization analysis results are given in two parts as design examples and a parametric study.

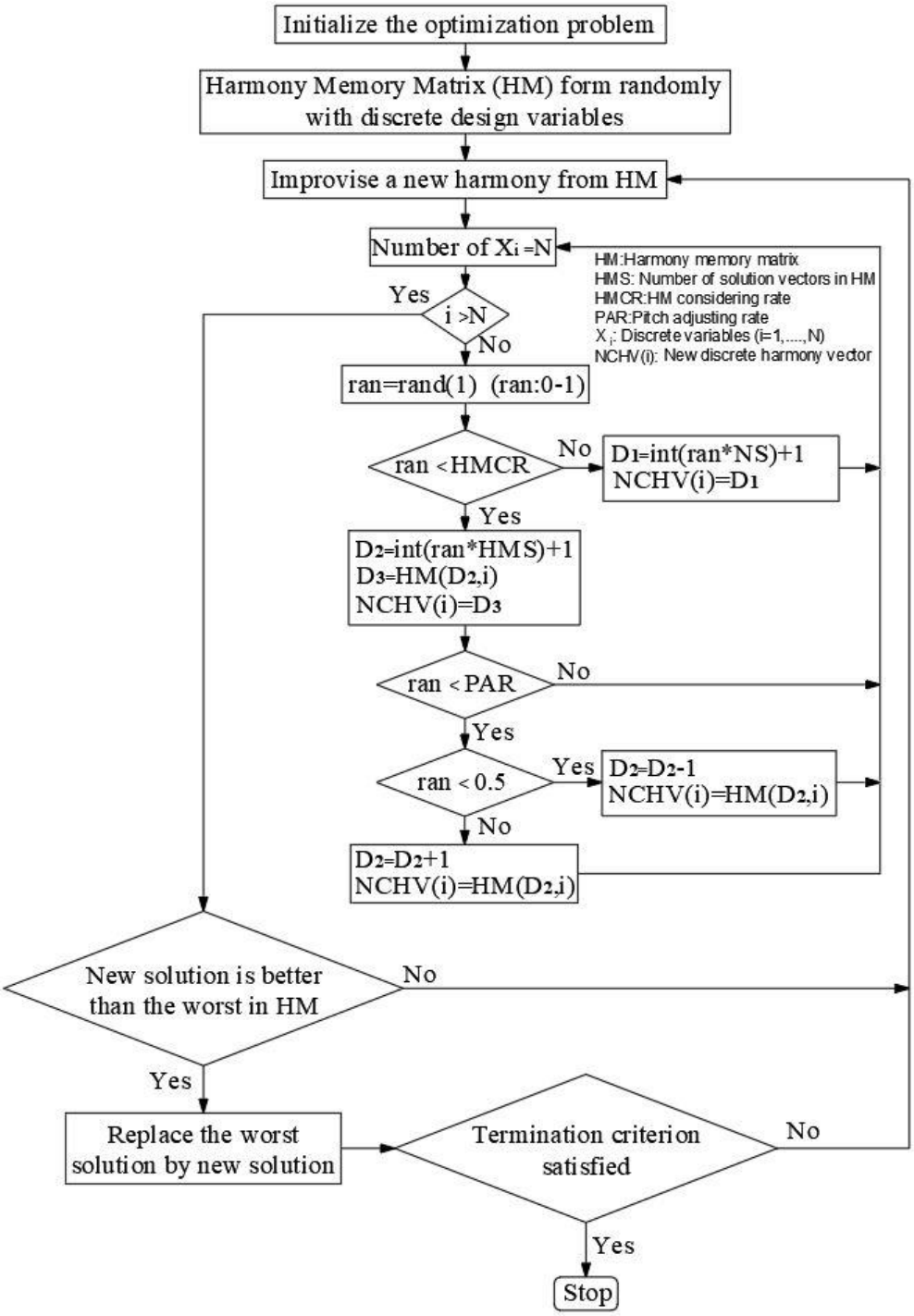

Fig. 2. Flowchart of harmony search algorithm for optimum design of a cantilever retaining wall.

3.1. Design Examples

The HSA has been used in finding the optimal weight of the cantilever retaining wall, which is given in Fig. 1, and five design examples have been represented proving that proposed the algorithm is efficient and productive. In the optimization analysis, after the wall weight has reached minimum value, the optimal wall weight has remained constant, even if values of the angle of internal friction and the unit volume weight have changed. This design, in which the optimal wall weight does not change with continued analyses, has been presented as design examples for each wall height.

In Table 3, input values, which have been used in the analysis, and the optimal wall dimensions, which have been obtained as results of analyses, are tabulated. Furthermore, revised lower and upper borders of design variables are given in this table. While each value of the wall height is given, some angle of internal friction value and unit volume weight are given as input parameters. This is due to the fact that the change values of unit volume weights during the optimal design do not affect significantly the optimal weight values, thus, γ_s= 18 kN/m^3 is chosen as the mean value.

In the design examples, after the optimal wall weight is obtained, the angle of internal friction value is taken which does not show any change in the optimal wall weight with continuing analyses. When Table 3 is examined, it is obviously seen that the optimal values of the retaining wall satisfy the lower and upper bounds determined with reference to the provision of American Concrete Institute Building Code Requirements for Structural (ACI 318-08, 2008) and LRFD Bridge Design Specifications (AASHTO, 2010).

Table 3. Input and optimum values for design examples.

Example No		1	2	3	4	5
Input Values	H (m)	4	5	6	7	8
	Ø (°)	30	35	40	40	40
	γ_s (kN/m^3)	18	18	18	18	18
Optimum Values	X_1 (m)	1.20	1.50	1.80	2.10	2.40
	X_2 (m)	0.204	0.225	0.306	0.315	0.36
	X_3 (m)	0.24	0.30	0.36	0.42	0.48
	X_4 (%)	2	2	2	2	2
Lower-Upper Bounds	X_1 (m)	1.2-4	1.5-5	1.8-6	2.1-7	2.4-8
	X_2 (m)	0.18-2.20	0.225-2.75	0.27-3.30	0.315-3.85	0.36-4.40
	X_3 (m)	0.24-0.64	0.30-0.80	0.36-0.96	0.42-1.12	0.48-1.28
	X_4 (%)	2-7	2-7	2-7	2-7	2-7

In Table 4, the values of the optimal weight and the sliding and overturning safety factors correspond to those optimal weights are evinced. For each optimal analysis, the lower bounds of both the safety factors of sliding and overturning have been accepted as 1.3 to ensure the stability conditions of the wall. It has been seen that the sliding safety factor is greater than the overturning safety factor for design examples. This can be due to the coefficient of friction has taken as equal to the angle of internal friction in the analyses.

Table 4. The optimum wall weight and the safety factors of sliding-overturning.

Example No	W_{wall} (kN)	$F_{s\,(\text{sliding})}$	$F_{s\,(\text{overturning})}$
1	34.2344	2.22	1.32
2	46.1475	2.66	1.40
3	59.4024	3.40	1.60
4	73.9991	3.07	1.47
5	89.9376	2.83	1.40

The changes between the wall weights (W_{wall}) and iteration numbers (iteration) are stated in Fig. 3 In the harmony search optimization, the wall weight decreases with the increase in the iteration numbers. It is clear that the optimal wall weight has been reached with approximately 150 iterations. Although 5000 iterations have carried out for each design, the optimal wall weight and design variables have been obtained with 150 iterations and remained unchanged anymore.

3.2. A Parametric Study

In the design optimization of cantilever retaining wall, the wall height, the unit volume weight of backfill and the angle of internal friction are crucial parameters affecting the optimal design. In this section, a detail parametric study carried out by using variable values of those parameters has been given in Table 2. While there is no effect of the unit volume weight change is sight, the influence of the wall height and the angle of internal friction change on optimal wall weight, on optimal design variables values, and on sliding and overturning safety factors were observed. As mentioned before since the change of the unit volume weight during the optimal design do not affect the optimal wall design weight, significantly, it is selected as 18 kN/m^3 as a mean value among 16 kN/m^3 to 20 kN/m^3.

In Fig. 4, as the wall height increases, the minimum wall weight increases rapidly. Also, there is an inverse proportion between the wall height and the internal friction angle for same wall height.

In Fig. 5, the relation between the base width (X_1) and the wall height (H) is defined by the coefficient of "α_B". The change between α_B and the wall height (H) is given for various angle of internal friction in the figure. From this figure, it is also clear that the slope of curve decreases with the raise of the angle of internal friction and that slope of curve is zero for Ø=40-45°. In Fig. 5, economic retaining wall design has been obtained for Ø=30-45°. While the base width may be taken about between 40% to 60% of the overall wall height in American Concrete Institute Building Code Requirements for Structural (ACI 318-08, 2008), this value may be chosen between 70% and 75% of the stem height according to LRFD Bridge Design Specifications (AASHTO, 2010) without paying attention for change of angle of internal friction. In return for this, the optimal wall design has been obtained for α_B=0.30 with parametric study for Ø>30°.

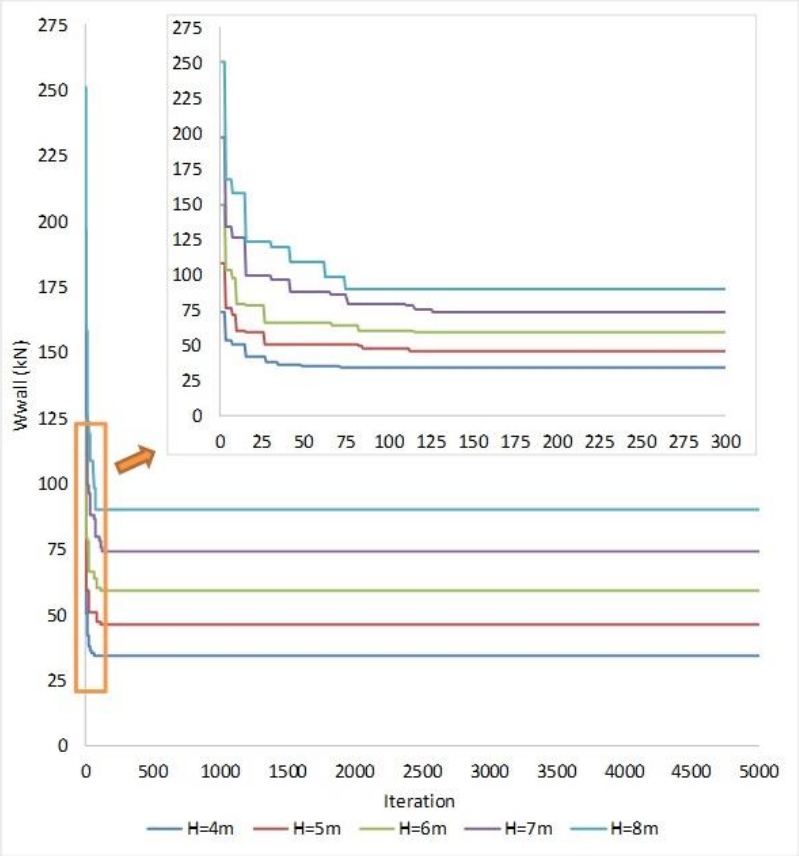

Fig. 3. Design histories of design examples.

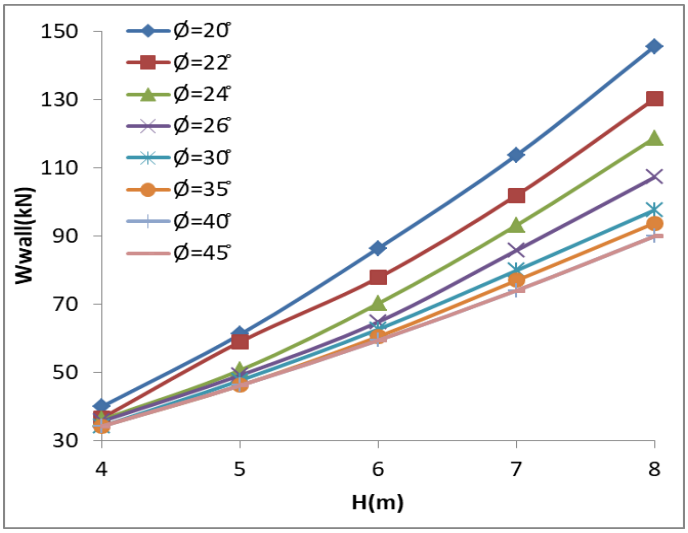

Fig. 4. The changes between the wall height and the minimum wall weight.

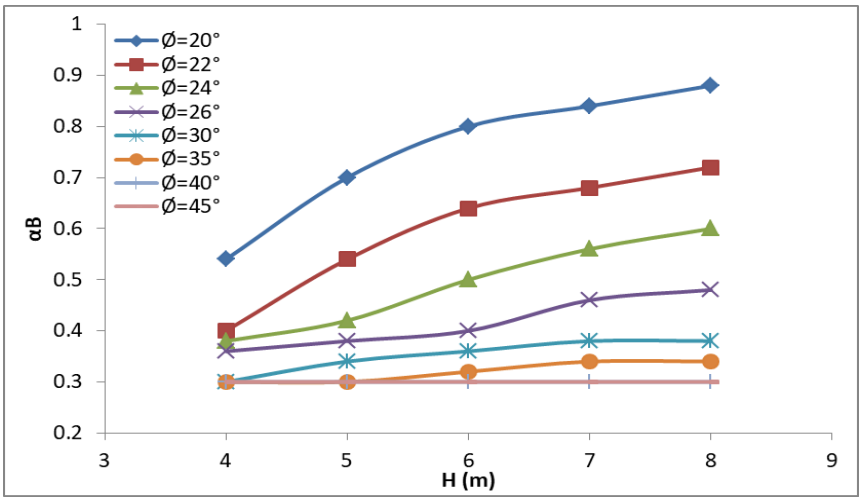

Fig. 5. The change between α_B and the wall heights.

The change of the toe width (X_2) according to the base width (X_1) is defined by the coefficient of "α_T". The values of α_T are given in Table 5 for the different values of the angle of internal friction and the wall heights. In Table 5, a non-proportional change between the base width (X_1) and the toe width (X_2) is evident. This non-proportional change is due to the randomization characteristics of the algorithm and the random search solution. For the toe width, 30% of length of base has been suggested according to above mentioned provisions and obtained α_T values less than this value. In analyses, it has seen that the coefficient of the thickness of base slab "α_D" has same ratio as 0.06 for all values of the wall heights and the angle of internal friction. Value of the angle of front face has been obtained as %2 (minimum value) like suggested in American Concrete Institute Building Code Requirements for Structural (ACI 318-08, 2008) and LRFD Bridge Design Specifications (AASHTO, 2010) in all analyses.

Table 5. The values of α_T.

Ø (°)	H=4m	H=5m	H=6m	H=7m	H=8m
20	0.15	0.15	0.15	0.15	0.15
22	0.15-0.21	0.15	0.15	0.15-0.17	0.15
24	0.15	0.15-0.17	0.15	0.15-0.17	0.15
26	0.15-0.21	0.17	0.15	0.15-0.17	0.15-0.17
30	0.15-0.17	0.19	0.15-0.21	0.19	0.15
35	0.25	0.15-0.23	0.17-0.21	0.17	0.15-0.17
40	0.25	0.23	0.17	0.15-0.17	0.15
45	0.25	0.23	0.17	0.17	0.17

In Table 6, for each wall height from 4m to 8m, the acquired the best and the worst design weights are designated for different values of the unit volume weight and the angle of internal friction. It is worthy to mention from this table that the worst design weights obtained for each wall height and each unit volume weight is reached at same angle of internal friction, which is Ø=20°. But, the best design weights for wall heights of 4m and 5m under all unit volume weights is achieved at Ø=30° and 35° the angle of internal friction values, respectively.

The most striking result can be deducted from this table is that the best design weights, for wall heights of 6m, 7m, and 8m under all unit volume weights, come into the view at the same angle of internal friction, which is 40°. This proves that the change of the angle of internal friction is more effective than change of the unit volume weight on the optimal wall weight. And also, it can be educed from this table that the higher the wall height, the more wall weight needed to attain the optimal design weight under each unit volume weight.

In the weight optimization of a cantilever retaining wall, the most desirable design is that the sliding and overturning constraints are close to limit safety factor and each other. So, if the safety factors of a design being close to limit value (1.3), the non-economical wall design is avoided.

In Table 7, among all optimal designs, those are presented whose sliding and overturning safety factors constraints are very close to each other. Thus, by use of those solutions, the most economical design can be obtained. This table may be useful in determining of approximate cost of a particular wall design with known wall dimensions and soil properties of backfill.

Table 6. Weight values of optimum design for different design parameters.

	γ_s =16 kN/m^3				γ_s =18 kN/m^3				γ_s =20 kN/m^3			
	Worst		Best		Worst		Best		Worst		Best	
H (m)	Ø (°)	W_{wall} (kN)	Ø (°)	W_{wall} (kN)	Ø (°)	W_{wall} (kN)	Ø (°)	W_{wall} (kN)	Ø (°)	W_{wall} (kN)	Ø (°)	W_{wall} (kN)
4	20	39.514	30	34.234	20	39.994	30	34.234	20	40.474	30	34.234
5	20	60.397	35	46.147	20	61.147	35	46.147	20	61.897	35	46.147
6	20	85.322	40	59.402	20	86.402	40	59.402	20	86.402	40	59.402
7	20	112.219	40	73.999	20	113.681	40	73.999	20	115.159	40	73.999
8	20	143.697	40	89.937	20	145.617	40	89.937	20	147.537	40	89.937

Table 7. Optimum wall design values in which sliding and overturning safety factor constraints are very close to each other.

H (m)	Ø (°)	γ_s (kN/m^3)	X_1 (m)	X_2 (m)	X_3 (m)	X_4 (%)	$F_{s\,(sliding)}$	$F_{s\,(overturning)}$	W_{wall} (kN)
4	22	16	1.60	0.336	0.24	2	1.3254	1.3559	36.6344
4	22	20	1.60	0.24	0.24	2	1.3146	1.3190	36.6344
5	24	16	2.00	0.3	0.30	2	1.3077	1.3402	49.8975
5	26	18	1.90	0.323	0.30	2	1.4423	1.3072	49.1475
6	26	18	2.40	0.36	0.36	2	1.3474	1.3776	64.8024
6	30	20	2.16	0.324	0.36	2	1.6634	1.3094	62.6424
7	26	18	3.22	0.483	0.42	2	1.3343	1.7091	85.7591
7	30	16	2.66	0.505	0.42	2	1.5912	1.4201	79.8791
8	26	16	3.84	0.653	0.48	2	1.3102	1.8498	107.2176
8	30	20	3.04	0.456	0.48	2	1.4694	1.3557	97.6176

In Fig. 6, soil types of compactness is studied by Peck (1974) have been given according to values of the angle of internal friction. By examining the graph plotted in Fig. 6, it is obvious that the optimal wall weight decreases rapidly for H=6-7-8 m. In increasing values of the angle of internal friction, it shows an approximately linear behavior for the other H values. It is obvious that the optimal design weights of the wall have been obtained for Ø=30° according to figure, which corresponds to the angle of internal friction of the medium dense sand.

Fig. 7 shows that the base width of the wall with increase the angle of internal friction decreases till Ø=30° for different wall height. Observation of a linear behavior after Ø=30° means that optimal values are obtained for approximately this angle of internal friction. According to figure, when there is a reduction of 66% from Ø=20° to Ø=30°, a decrease of 21% is observed after Ø=30° for H=8 m.

In Fig. 8, nearly linear behavior in increase of the values of the angle of internal friction has been seen after especially Ø=30°. Since the toe with has been defined as depend on the base width given in Table 1, curve of change the toe width is similar to curve of change the base width in varied wall height.

Change of the thickness of base slab depend on the wall height has been dedicated with the angle of internal friction in Fig. 9. As regards figure, increasing of the angle of internal friction has not affected the thickness of base slab. for different values of all wall height, fixed values of X_3 have been achieved, even if the angle of internal friction changes; for instance, X_3 is equal to 0.24 m for H=4 m or 0.30 m for H=5 m. However, same angle of front face of the wall has been obtained as X_4=2% for each different wall design during the parametric study. Because, values of the angle of front face have remained constant for diversified values of design parameters like the wall height, the unit volume weight and the angle of internal friction, it is concluded that X_4 is not effective on wall design.

Results from the optimization analyses show that change of the angle of internal friction has an important influence on safety factors of sliding and overturning. The changes between the angle of internal friction and sliding and overturning safety factors have been tabulated in Figs. 10 and 11, respectively.

In Fig. 10, as the angle of internal friction increase, the safety factor has gone up especially after Ø=30°. The sliding safety factor has increased by an average of 52% with higher values of angle of internal friction for H=4 m and Ø=35°, 40°, 45°. In this case, since the optimal wall

weight has been attained at Ø=30° and not to alter for other angle of internal friction, the optimized-economic wall design cannot be achieved after Ø=30°.

When the Fig. 11 is investigated, the effect of the angle of internal friction change on the overturning safety factor has been seen clearly. As the safety factor decreases till Ø=30°, it increases after this value for each wall height. Since this behavior has not any impact on the optimal wall weight, it is obvious that economic wall design cannot be achieved for higher the angle of internal friction like 35°, 40°, 45°.

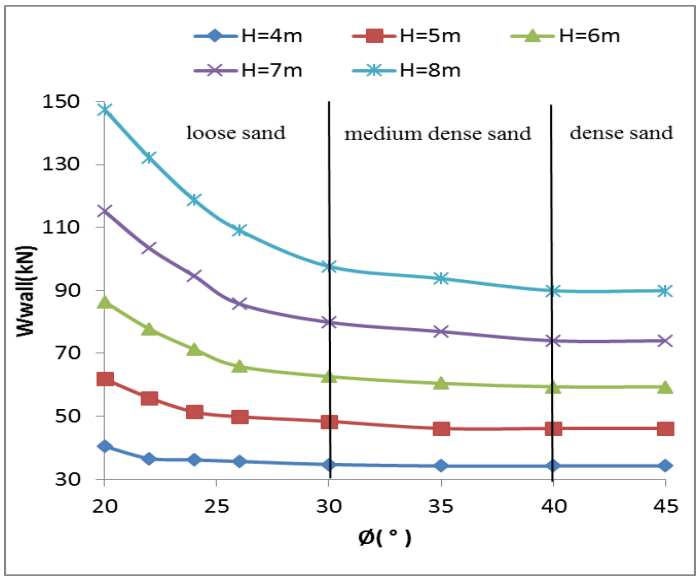

Fig. 6. The changes between the wall weight and the angle of internal friction.

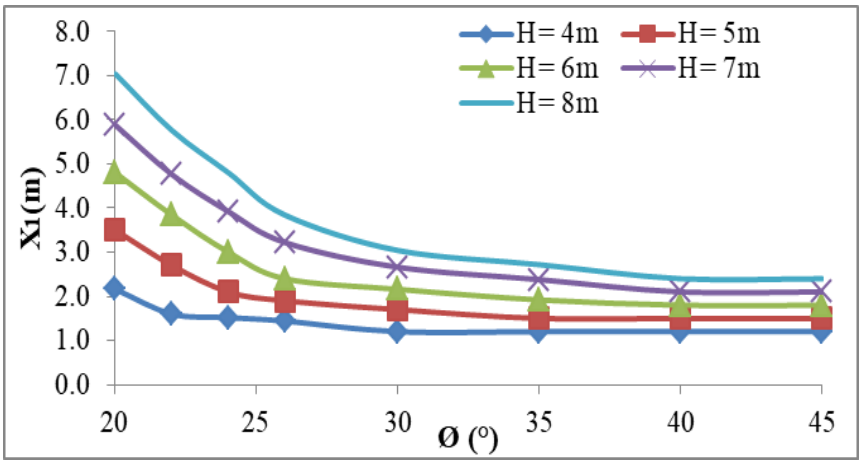

Fig. 7. The change between the base width and the angle of internal friction.

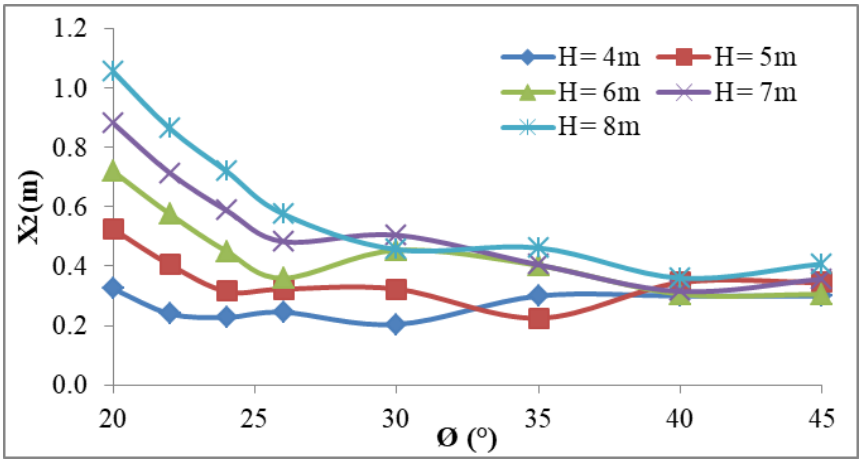

Fig. 8. The change between the toe width and the angle of internal friction.

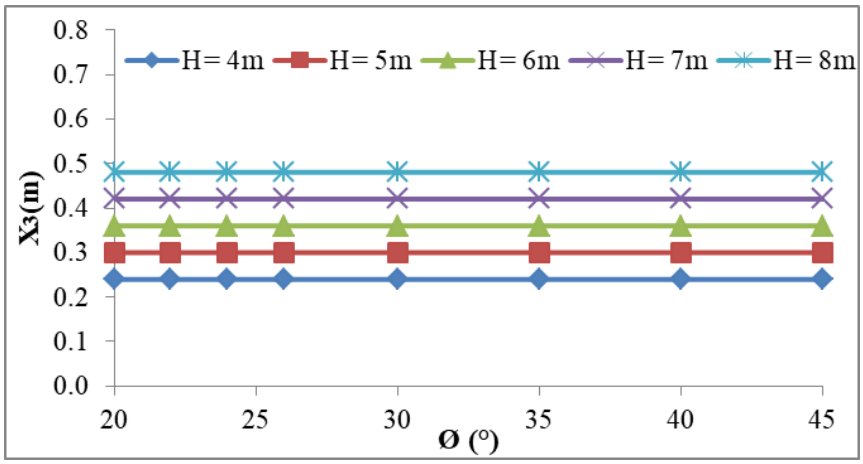

Fig. 9. The change between the thickness of the base slab and angle of internal friction.

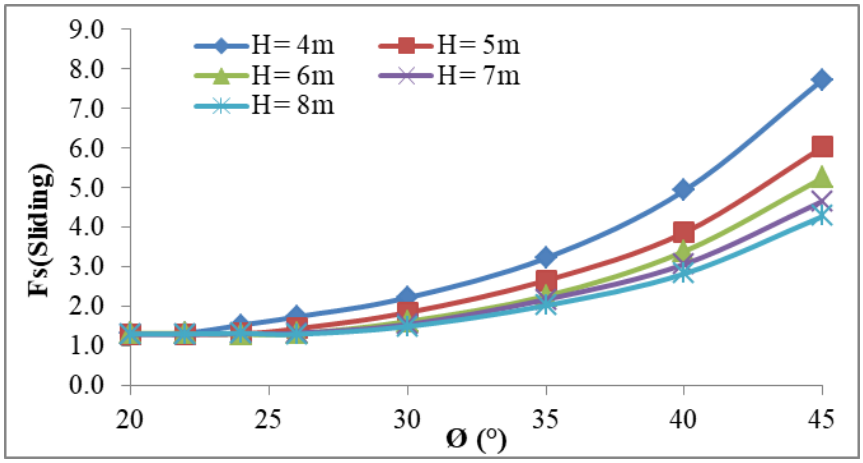

Fig. 10. The change between sliding safety factors and angle of internal friction.

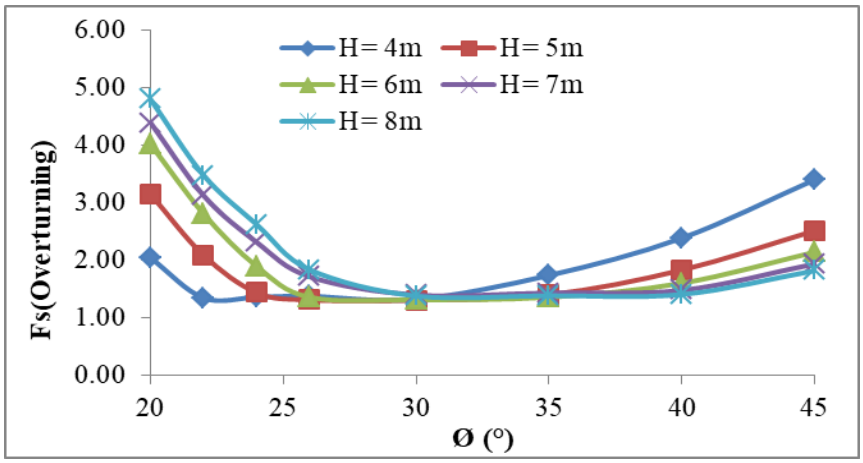

Fig. 11. The change between overturning safety factors and angle of internal friction.

4. Conclusions

In the current paper, the optimization study and a detail parametric study has been presented for the optimal design of a cantilever retaining wall by using the harmony search algorithm, which is one of the recently improved and successful optimization methods. The optimal wall dimensions leading the minimum wall weight have been found. The wall weight is treated as the objective function. In the design problem, due to the fact that safety factors against sliding and overturning are taken as constraints, the stability of the cantilever retaining wall provides for the determined optimal weights. In addition, geometric constraints due to the wall geometry have been considered in the optimal design of cantilever retaining wall. The optimal wall dimensions obtained have been satisfied the upper and the lower limits given for the design variables. The optimal weight of the wall has been

obtained in less time and with less iteration compared with the traditional design of the cantilever retaining walls.

In the parametric study, the wall height and the angle of internal friction have found to be quite effective in the design of cantilever retaining walls. Generally, the unit volume weight values vary in a very limited range according to type of soils, for instance, value of the unit volume weight may be considered as 20 kN/m^3 for gravel and as 23 kN/m^3 for silty sand and gravel (Das, 2008). Therefore, obtained results show that unit volume weight change does not affect effectively design in this study which values of the unit volume weight have been taken between 16-20 kN/m^3.

In analyses, because soil type used in optimization analyses have been considered as sand, cohesion value of soil has been taken zero for the optimal cantilever retaining wall design. In general, the optimal wall weights have been attained for Ø=30° which correspond to the angle of internal friction of medium dense sand. In this point, because the compactness of soil change, from loose to medium density, it is reasonable to obtain optimal values in this value. In other words, while the weight of wall rapidly declines (34%) in the range of loose-medium dense sand (Ø<30°), it is seen that a less weight decrease of wall (8%) in the range of medium dense-dense sand (30°<Ø<40°) for H=8 m.

In this study, selection of wall dimensions has been conducted according to provisions of American Concrete Institute Building Code Requirements for Structural (ACI 318-08, 2008) and LRFD Bridge Design Specifications (AASHTO, 2010). On the other hand, the optimum wall dimensions obtained in the optimization analyzes differ from suggested wall sizes according to the ACI 318-08 (2008) and AASHTO (2010) which are independent of variable value of internal friction. This result shows that, it is necessary to take into consideration the soil property such as the internal friction angle in the design of cantilever wall.

Eventually, this study has shown that such heuristic methods may be used in finding the optimal solutions for geotechnical engineering problems. The harmony search algorithm and its improved versions may be applied easily used in any similar future research. In this way, it is possible to obtain pre-dimension guides which help to determine the optimal wall dimensions and to provide safe and economic design. Because the proposed optimization algorithm is simple mathematically, application of the algorithm is easier than other traditional optimization methods. As a future work, the algorithm may be used effectively and reliably in the design of the cantilever retaining wall for different cases such as sloping filling, surcharge load, groundwater, multilayer soil and cohesive soil.

Acknowledgements

In this study, results of a part of continuing doctoral thesis has been submitted and also it is supported by Scientific Research Projects Coordination Units of Selçuk University Research Funding (BAP-17401107) which are gratefully acknowledged.

REFERENCES

ACI 318-08 (2008). ACI Committee 318, Building Code Requirements for Structural Concrete. American Concrete Institute, USA.

AASHTO (2010). American Association of State Highway and Transportation Officials LRFD Bridge Design Specifications, USA.

Akın A, Saka M (2010). Optimum design of concrete cantilever retaining walls using the harmony search algorithm. *Proceeding of 9th International Congress on Advances in Civil Engineering Civil-Comp Press*, 27-30.

Ayvaz MT, Elçi A (2013). A groundwater management tool for solving the pumping cost minimization problem for the Tahtali watershed (Izmir-Turkey) using hybrid HS-Solver optimization algorithm. *Journal of Hydrology*, 478, 63-76.

Bekdaş G, Nigdeli SM (2016). Optimum design of reinforced concrete columns employing teaching learning based optimization. *Challenge Journal of Structural Mechanics,* 2(4), 216-219.

Camp C, Akin A (2012). Design of retaining walls using big bang–big crunch optimization. *Journal of Structural Engineering*, 138(3), 438-448.

Ceranic B, Fryer C, Baines RW (2001). An application of simulated annealing to the optimal design of reinforced concrete retaining structures. *Computers and Structures*, 79(17), 1569-1581.

Chau KW, Albermani F (2003). Knowledge-based system on optimal design of liquid retaining structures with genetic algorithms. *Journal of Structural Engineering*, 129(10), 1312-132.

Cheng YM (2009). Modified Harmony Methods for Slope Stability Problems. *In: Geem Z.W. (eds), Music-Inspired Harmony Search Algorithm Studies in Computational Intelligence*, Springer, Berlin, 141-162.

Cheng YM, Li L, Fang SS (2011). Improved harmony search methods to replace variational principle in geotechnical problems. *Journal of Mechanics*, 27(1), 107-119.

Fattahi H (2015), Prediction of slope stability state for circular failure: a hybrid support vector machine with harmony search algorithm. *International Journal of Optimization in Civil Engineering*, 5(1), 103-115.

Gandomi AH, Kashani AR, Roke DA, Mousavi M (2015). Optimization of retaining wall design using recent swarm intelligence techniques. *Engineering Structures*, 103, 72-84.

Geem ZW, Kim JH, Loganathan GV (2001), A new heuristic optimization algorithm: harmony search. *Simulation*, 76(2), 60-68.

Geem ZW, Lee KS, Park Y (2005), Application of harmony search to vehicle routing. *American Journal of Applied Sciences*, 2(12), 1552-1557.

Keskar AV, Adidam SR (1989), Minimum cost design of a cantilever retaining wall. *Indian Concrete Journal*, 63 (8), 401-405.

Khajehzadeh M, Taha MR, El-Shafi A, Eslami M (2010). Economic design of retaining wall using particle swarm optimization with passive congregation. *Australian Journal of Basic and Applied Sciences*, 4(11), 5500-5507.

Khajehzadeh M, Taha MR, El-Shafi A, Eslami M (2011). Economic design of foundation using harmony search algorithm. *Australian Journal of Basic and Applied Sciences*, 5(6), 936-943.

Khajehzadeh M, Eslami M (2012). Gravitational search algorithm for optimization of retaining structures. *Indian Journal of Science and Technology*, 5(1), 1821-1827.

Lee KS, Geem ZW, Lee, SH, Bae KW (2005). The harmony search heuristic algorithm for discrete structural optimization. Engineering Optimization, 37(7), 663-684.

Matlab: https://www.mathworks.com/products/matlab.html

Molina-Moreno F, García-Segura T, Martí JV, Yepes V (2017). Optimization of buttressed earth-retaining walls using hybrid harmony search algorithms. *Engineering Structures*, 134, 205-216.

Peck RB, Hanson WE, Thornburn TH (1974). Foundation Engineering. Wiley, New York.

Rhomberg, EJ, Street WM (1981). Optimal design of retaining walls. *Journal of the Structural Division*, 107(5), 992-1002.

Saka MP, Çarbaş S (2009). Optimum design of single layer network domes using harmony search method. *Asian Journal of Civil Engineering (Building and Housing)*, 10(1), 97-112.

Sheikholeslami R, Gholipour Khalili B, Zahrai SM (2014). Optimum cost design of reinforced concrete retaining walls using hybrid firefly algorithm. *International Journal of Engineering and Technology*, 6(6), 465-470.

Talatahari S, Sheikholeslami R (2014). Optimum design of gravity and reinforced retaining walls using enhanced charged system search algorithm. *KSCE Journal of Civil Engineering*, 18(5), 1464-1469.

Temür R, Bekdaş G (2016). Teaching learning-based optimization for design of cantilever retaining walls. *Structural Engineering and Mechanics*, 57(4), 763-783.

Uray E, Çarbaş S, Erkan İH, Tan Ö (2015). Optimum design of concrete cantilever retaining walls with the harmony search algorithm. *Proceeding of 6th Geotecnichal Symposium, Cukurova University*, Adana, Turkey.

Yepes V, Alcala J, Perea C, González-Vidosa F (2008). A parametric study of optimum earth-retaining walls by simulated annealing. *Engineering Structures*, 30(3), 821-830.